MECHANISTIC MODELS OF UNCONVENTIONAL RESERVOIRS

By

POUYAN LIALEKOL, EBRAHIMI

Bachelor of Science in Petroleum Exploration Engineering
Petroleum University of Technology
Abadan, Iran
2008

Master of Science in Petroleum Exploration Engineering
Sahand University of Technology
Tabriz, Iran
2011

Submitted to the Faculty of the
Graduate College of the
Oklahoma State University
in partial fulfillment of
the requirements for
the Degree of
MASTER OF SCIENCE
July, 2015

MECHANISTIC MODELS of UNCONVENTIONAL

RESERVOIRS

Thesis Approved:

Dr. Priyank Jaiswal

Thesis Adviser

Dr. Michael Grammer

Dr. Jim Puckette

ACKNOWLEDGEMENTS

I would like to express my gratitude to faculty, staff, and students in the Boone Pickens School of Geology; all have contributed for making my stay at Oklahoma State University a wonderful life experience.

I wish to sincerely thank my adviser, Dr. Priyank Jaiswal who helped me during my studies and supported me financially. It was such an honor to have worked and interacted with all members of my thesis's committee, Drs. James Pucktte and Michael Grammer.

I would like to express my sincere appreciation to Drs. Mohamed Abdelsalam and Estella Atekwana for their mentoring and encouragement which made me complete my MS degree. They really care about all students. As William Shakespeare says:

"I can no other answer make, but, thanks, and thanks."

I would like to thank my friends at OSU, Mercy Achang, Beth Vanden Berg, Muhammad Salman Abbasi, Afshin Aghayan, Iftekhar Alam, Khemraj Shukla, and Andrew Kaumwehe, who always were supportive. Without their help, I could have not finish my thesis.

Lastly, I would like to appreciate my family, they are always in my heart. All success that I have in my life is because of my mother, father and my sisters, especially my oldest sister, Simin. I just can only say, I love them.

Name: POUYAN LIALEKOL, EBRAHIMI

Date of Degree: JULY, 2015

Title of Study: MASTER OF SCIENCE

Major Field: GEOLOGY

Abstract: Rock physics models are mathematical relations between porosity, composition and elastic properties of a rock. Unlike in conventional silisiclastic rocks where seismic-to-rock properties are predicted successfully by rock physics models, their application in unconventional reservoirs such as shale, hydrate and carbonates is not fully understood. In light of the vast untapped potential of unconventional resources, their exploration will be easier if a suitable rock physics models become available for quantitative interpretation of seismic data. In this thesis generic, rock physics models that were developed for conventional siliciclastic systems have been used to infer rock properties such as porosity, composition, fluid saturation and pore pressure in shale, gas hydrates and carbonates. Results indicate that elastic properties of these rocks including shale and gas hydrates which can be viewed as grain assemblages can be best predicted by Hashin Shtrikman bounds. For rocks with non-spherical pores and a rather unified matrix such as carbonates where grain-to-grain contacts are not very clear, the Kuster and Toksoz model provide a good description of their dry elastic properties.

TABLE OF CONTENTS

LIST OF TABLES

Table Page

LIST OF FIGURES

Figure Page

CHAPTER I

INTRODUCTION

Hydrocarbon reservoirs can be generally divided into two categories, 'conventional' and 'unconventional' (Zou et al., 2013). The term "unconventional" refers to reservoirs where development demands advanced engineering such as gas/steam injection, hydraulic fracturing and horizontal and multilateral well placement (Seljom, 2010). The exact definition of an unconventional reservoir is lacking but it seems like the categorization is technology dependent (Gordon, 2012). It is possible that as the newer technologies become more and more mundane, certain reservoirs may move from the unconventionals to the conventional category in the near future (McGlade et al., 2013). Although more than two-third of worldwide hydrocarbon reserves can be accredited to unconventionals (Figure 1), extreme caution is required in their development due to their high-risk nature (Cipolla et al., 2011). At present, unconventional reservoirs are divided into seven main categories: tight-sandstone, coalbed methane, shale, carbonate, metamorphic rocks, heavy oil and bitumen, and gas hydrate (Zou, 2012). This classification is generic and varies from one company to another.

Unconventional resources such as the Woodford Shale and the Mississippian limestone are greatly sought after in the mid-western United States. Geophysics has not played a strong role in development of these reservoirs. The location (depth and spatial extent) of these reservoirs is known from decades of developmental work related to other conventional reservoirs in the area. Lately operators have started realizing that reservoir heterogeneity significantly effects

production economics and a detailed understandings of reservoir conditions is required before landing the well. Seismic data can serve the needs (Rich and Ammerman, 2010), their velocities contains important information about the petrophysical properties of the rock. However, methods to translate seismic velocities into rock and fluid properties in shales and carbonates are not well developed.

Research on development of unconventional gas hydrate reservoirs are being actively pursued by many countries including the United States. Gas hydrates are deposits of frozen gas in the near-seafloor sediments. In oceans, the geothermal gradient and seafloor depth define a zone of stability (gas hydrate stability zone; GHSZ), within which gas, mostly methane, can exists with water in crystalline arrangements (Buffett, 2000). Growth habits of hydrate within the GHSZ are varied: in coarse-grained sediments, they can reside in pore-spaces, support the sediment framework as load-bearing grains, or bind the sediment grains as cement; in fine-grained sediments, they can create or occupy veins and fractures; on or near the seafloor they can form massive mounds (Kvenvolden, 1994; Max, 2003). As a solid, $1m^3$ of hydrate can contain up to $164m^3$ of methane at Surface Temperature and Pressure (STP) (Sloan and Koh, 2007), which is viewed as a potent greenhouse gas as well as a source of energy (Svensen *et al.*, 2004), energy resources (Collett, 2002), and seafloor stability (Rothwell *et al.*, 1998). The most common way of locating a GHSZ is finding high seismic velocity zones that end at a high reflection interface (known as the Bottom Simulating Reflection, BSR), which is created when the hydrate becomes unstable and changes to the gas phase. Like other unconventional systems, estimating petrophysical properties of hydrate from seismic data is in an exploratory stage.

1.1 Use of seismic data in unconventional reservoirs

Beyond using seismic data for time/depth mapping it is not uncommon to design need based analysis methods for more quantitative facies identification. Ebrahimi and Jaiswal (2014) used a

directional filter on seismic cross-section images of the Fareo-Shetland basin to enhance sub-basalt dipping stratigraphy. Ebrahimi et al. (2014) integrated different seismic attributes (such as curvature, similarity, polar dip, RMS) using Geographic Information Systems (GIS) to highlight fracture systems within a sandstone reservoir in Venezuela. Bahorich and Farmer (1995) used the coherence attribute to reveal a fault surface where there is not any fault plane reflections within a 3D seismic data. Lonergan and Cartwright (1999) used the contrast in density of faults within different subdomains to explore subtle sandstone targets in mudstone-dominated deep-water systems of Alba Field. Barber and Marfurt (2010) used Sobel filter and spectral decomposition to highlight otherwise unresolvable depositional sandstone channels in the Anadarko Basin in west-central Oklahoma.

Besides mapping and facies classification, seismic data have also been used for extracting petrophysical properties of reservoirs. However, examples are mostly of in conventional sandstone formations. For example, Ryseth et al. (1998) used 3D seismic data integrated with geological well data (thickness and depositional systems of geological formations) to correlate elastic velocities and sandstone proportion within the Ness Formation in the Oseberg field. Hamdi and Smith (1982) established a model based on Biot's equation to predict permeability of a seafloor sediment using a wide range of seismic velocities; Biot's equation describes the change in bulk volume by changing pore pressure (Biot, 1955). Eberhart-Phillips et al. (1989) designed laboratory experiments on sandstone rocks and found an empirical relation between seismic velocities and rock characteristics such as effective pressure[1], porosity and clay content. Although their equation cannot exactly describe the sonic velocities of all sandstone samples, the fit is reasonable and may help to estimate sonic velocities. Domenico indicated that Poisson's ratio (division of lateral expansion to axial compression under uniaxial compressional stress (Gercek, 2007), which has direct relation with the ratio of compressional to shear waves (Vp/Vs)) of rocks,

[1] difference between confining pressure and pore pressure

depends on their mineralogies. Since dominant mineralogy in sandstone and limestone are respectively quartz and calcite, he used their Poisson's ratios to distinguish them. He also found an empirical formula to relate sonic velocities to porosity.

In addition to matrix composition, pore fluid also affects the sonic velocities. Standard condition of the reservoir conditions (pressure, temperature, and water salinity) change pore fluids' elastic moduli and eventually vary the elastic moduli and elastic velocities of the whole rock. Gassmann's equations contribute in finding the amount of changes in elastic velocities and bulk density due to fluid saturations under reservoir condition (Gassmann, 1951; Kumar et al., 2006). Despite the popularity of Gassmann's equations in interpretating seismic data, they will not provide the exact solution due to their several assumptions including: 1) equilibrated pore pressure between pores, 2) isotropic[1] porous material with a single solid material (monomineralic), 3) homogeneous and well-connected pores which are fully filled with a nonviscous fluid, 4) system is undrained or closed, 5) no reaction between fluids and rock frame (Adam et al., 2006). Due to the first assumption, his equations are not valid for high frequency[2] (>100 HZ) waves. Because after propagating high frequency waves, the fluid within porous media does not have to be relaxed or equilibrated (Mavko et al., 2009).

Petrophysical properties and rock composition can be related to their elastic velocities more generally using mathematical models collectively known as Rock Physics (Eberli et al., 2003; Mavko et al., 2009). Applying appropriate rock physics models in each type of rock enables seismologists to quantitatively interpret sonic velocities from seismic surveys and sonic logs (Avseth et al., 2005; Dai et al., 2004; Jaiswal et al., 2014). In this project, rock physics models that were designed for conventional systems can also be applied to many unconventional systems.

[1] Segments showing the same responses when measured

[2] Rate of occurrences of a repeating event per unit time

This is demonstrated using data from a) the Woodford Shale in the McNeff 2-28 Well, Grady County, Oklahoma; b) gas hydrate deposits from NGHP-01-10, Krishna-Godavari Basin, India; and c) Mississippian carbonate reservoirs from the Blackbird 4-33, Osage county, Oklahoma.

CHAPTER II

BACKGROUND

The ultimate goal of constructing a mechanistic models of rocks is to be able to replicate their field seismic velocities. As opposed to data-based empirical relations, mechanistic models are physics-based and have better predictive abilities. The best example is the Wyllie et al. (1958) time average equation which was developed for conventional siliciclastic rocks. Sholl and Hart (1993), Wood et al. (1994), and Korenaga et al. (1997) successfully applied Wyllie's equation to estimate gas hydrate saturation in sand. Although Wyllie's equation was useful, its physical basis is weak; it cannot be justified under high or low porosity (Dvorkin and Nur, 1998) or highly heterogeneous material with near-zero permeability (Bathellier et al.; Goodway et al., 2010; Koesoemadinata et al., 2011).

2.1 Rock physics basics

Rock physics refers to a sub-discipline which deals with mathematical expressions that relate elastic velocities with composition and petrophysical properties of rocks. The elastic velocities have two main dependents – bulk density and elastic moduli (Equation 1). Elastic modulus is a measure of resistance that a material offers against deformation by an external force, such as the propagating seismic wavefield. Mechanically, two types of moduli can be defined. First is the bulk modulus and second is shear modulus, which is also known as the modulus of rigidity. Respectively, they are the strength of a material against distortion by uniform pressure and shear stress (Fossen, 2010; Price and Cosgrove, 1990). Elastic moduli of a porous rock depend on a

number of parameters such as their mineralogical composition, porosity and grain shape and their connectivity; of these, porosity is the most dominant property.

$$V_p = \sqrt{(K + 4/3\, G)/\rho}, \qquad V_s = \sqrt{G/\rho} \qquad \text{Eq. 1}$$

In Equation 1, Vp is compressional velocity, Vs: shear velocity, K: bulk modulus, G: shear modulus, ρ: density

From a rock physics perspective, for a multi-mineral rock, the following are needed for estimation of their elastic velocities: (1) fractions of different phases (minerals and pore fluids) inside the mixture; (2) the elastic moduli (bulk and shear modulus) of individual phases, and (3) the arrangement of these phases related to each other (Mavko et al., 2009). Grain arrangement is a critical factor for rock properties. Sometimes, it is the geometric arrangement of the grains which can separate an unconventional reservoir from a conventional one even though the mineralogy may remain the same. The geometric arrangement, i.e., grain packing also controls the porosity. In Figure 2, representative grain arrangement are shown for one conventional and three different unconventional rock types considered in this thesis. Figure ‘a’ to ‘d’ respectively present homogenous, inhomogeneous, gas hydrate saturated and carbonate rocks and their schematic diagrams are shown in the same order from ‘e’ to ‘h’. As depicted in the Figure 2.a, within a homogenous rock all grains have almost the same size. However, as shown in the Figure 2b, the shale rock has minerals with different dimensions. In Figure 2c, the gas hydrate is acting like an additional mineral grain in the matrix. In Figure 2d, the carbonate rock appears as having a frame (as opposed to grains juxtaposed against each other) with several types of pore shapes. In the context of rock physics, it is not possible to incorporate material heterogeneities “as is” in a mathematical model. The key is to simplify grain arrangement while honoring the dominant form of heterogeneity at the same time.

Although there are a number of ways to estimate the elastic moduli of a rock for a given porosity (Mavko et al. 2009), in context of this paper the Hashin-Shtrikman (HS) bound are most relevant. For a given porosity, depending on how easily the pores can be deformed, i.e., whether they are soft or tight, the HS bounds provide the maximum and the minimum possible rock stiffness. Application of HS bounds assume that the rock is isotropic and quasi- homogeneous. Isotropy implies that deformation (strain) is the same in all directions for the same stress. Quasi-homogeneous implies an individual element is representative of the group material properties. The concept of quasi-homogeneity is best illustrated by assuming that the material is comprised of multi-dimensional spheres that pack the space completely. Each sphere consists of an outer shell which surrounds an inner sphere is composed of a different material. The volumetric ratio of the two material is constant in all spheres (Figure 3). When the outer shell is a softer material, it can be shown using the continuum mechanics that the deformation is large for the same stress than at higher porosity. This simulates a rock with minimum possible stiffness and the deformation corresponds to presence of "soft" pores. The trajectory created in the moduli-porosity space with this material configuration yields the lower HS bound. Similarly the upper HS bound can be conceived (Figure 4).

HS bounds are used for grain mixing under different types for pore conditions. For example, when sediments are uncompacted, such as in the near-surface setting (marine or terrestrial), the pores are easily deformable. The lower HS bounds can be used to simulate such rock conditions (Helgerud 1999). On the other hand when the sediments are deeply buried and compacted, they are lithified and the pores are tight and the upper HS bounds can be used (Mavko et al., 2009). To illustrate the application of rock physics on unconventional reservoirs, three well-log datasets are being used in this research with the goal of replicating the observed elastic velocities (V_P and V_S) using mechanistic grain and fluid arrangements. The datasets are from a) Woodford Shale reservoir, McNeff 2-28 well in Grady County, OK; b) hydrate bearing reservoirs from NGHP-01-

10, Krishna-Godavari Basin, India; and c) Mississippian carbonate from the Blackbird 4-33, Osage County, Oklahoma.

2.2 Shale Reservoirs:

Shale could be hydrocarbon-rich fine- to very fine- grained sedimentary rock (Grainger, 1984) with extremely low permeability. As in the case of siliciclastic reservoirs, where sonic velocities from dipole logs and field surveys can be mapped to their composition and petrophysical properties, whether the same can be done in shale is not fully explored (Peebles, 2012). In contrast to siliciclastics, experimental studies in shale are not straightforward mainly due to small particle size of matrix constituents and ease of reaction with materials which are commonly used for lab measurements (Handwerger et al., 2011; Josh et al., 2012; Kuila and Prasad, 2013). Predicting shale rock properties with seismic has been a long-standing challenge (Dowdell et al., 2012; Sukmono, 2010). The key character of the shale reservoir under investigation in this study is its heterogeneity and compact nature.

Most shales are fairly heterogeneous compositionally. They are contain of quartz, clays, carbonates, feldspars, apatite, pyrite, and organic matter (OM) in varying proportion. From a rock physics perspective, the most peculiar type of heterogeneity is the OM which can appear in many styles within the rock. It can appear as a very thin lamina between grains due to post-depositional compaction or as residue from oil migration (Curtis et al., 2012a; Sondergeld et al., 2010). They are also found to be encasing small particles of inorganic matter (Curtis et al., 2012b). Recent ion beam milling and scanning electron microscopy (SEM) discovered that OM also has internal porosity which may or may not be connected to the rock porosity, thus serving as a source of secondary porosity (Dahl et al., 2012; Loucks et al., 2009; Reed et al., 2012). Pores within the OM can contain free oil and gas (Jarvie, 2012). While other components in a shale rock can be clearly classified belonging to the solid matrix or the pore-fluid, it is not very clear from literature

how OM needs to be treated. Thus, the key to a successful rock physics modeling in shale is being able to appropriately place the OM within the rock (Kleineidam et al., 1999).

The Woodford Shale investigated in this study is from 10,280ft to 10,450ft. At that depth it is expected to be highly compacted, implying that the pores are stiff and that a change in overburden pressure may not severely alter the porosity as for the unconsolidated rocks. The moduli-porosity relation for compacted rocks can be best approximated by the upper HS bounds, also known as the stiff sand model. Till now, the stiff sand model has been generally applied to isotropic and consolidated (under confining pressure) sandstones which are expected to comprise randomly-packed spheres with well connected pores. The Woodford Shale is siliceous in nature. An SEM image of the Woodford Shale from a location near the McNeff well (Caldwell, 2012) supports that kind of grain arrangement.

2.3 Gas Hydrate Reservoirs:

Gas hydrates are ice-like substances that contain gas molecules held by cages of water molecules that are stable within a short range of pressure and temperature. It has been estimated that over 15 trillion TOE (Tons of Oil Equivalent) of gas hydrate exists on our planet (Makogon and Cieslewicz, 1981). The pressure-temperature stability field for hydrate exists in marine and permafrost environments (Kvenvolden, 1993; Makogon and Cieslewicz, 1981). Hydrates precipitates from an oversaturated solution. Therefore, depending on the availability of space and ease of reactions, they have many different forms. Within coarse-grained sediments, they can be suspended in the pore fluid (Kida et al., 2009), hereafter referred to as the pore-filling model, or act like an additional mineral grain in the matrix (Winters et al., 2004), referred to as the load-bearing model. They can also develop as cement at grain contacts (Dvorkin and Nur, 1996). In fine grained sediments, hydrate can also create and fill fractures (Daigle and Dugan, 2010b; Hutchinson et al., 2008) or develop as nodules (Bohrmann et al., 1998).

Regardless of their accommodation style, presence of gas hydrates within a rock increases the elastic velocities. The increase depends on both the form of the hydrates and their saturation (Jakobsen et al., 2001). In the literature, effects of hydrate in pores and matrix and as cement on elastic velocities has been adequately addressed (Dvorkin and Nur, 1996; Dvorkin et al., 1994; Helgerud et al., 1999). However, the effect of hydrates in fractures on elastic velocities is somewhat less understood although it is found widely in nature. The main reason is difficulty in reproducing this growth style in physical scale experiments. In particular, this growth style was found in the Krishna Godavari (KG) basin, where one of the biggest hydrate discovery was made. The hydrate were found in fractured sediments. Till now, at least three different mechanistic models (Cook et al., 2010; Ghosh et al., 2010; Lee and Collett, 2009) have been proposed to explain the elastic velocities. None of them could simultaneously match the velocities and the saturation. However, using a combination of two rock physics models, loadbearing and HS, it can be shown that the elastic velocities and the saturation are appropriately predicted.

2.4 Carbonate Reservoirs:

Carbonate rocks are a category of sedimentary rocks which contain carbonate minerals such as calcite ($CaCO_3$) and dolomite ($CaMg(CO_3)_2$) (Palaz and Marfurt, 1997). More than 50% of oil and gas in the world is produced from carbonate reservoirs (Xu and Payne, 2009). Application of seismic in quantitative interpretation of carbonate reservoirs is still in an exploratory stage. The main reason is because the relation of rock composition to sonic velocity in carbonates is not well understood (Xu and Payne, 2009). For example, in siliciclastic rocks, increasing porosity decreases sonic velocity (Mavko et al., 2009), but in carbonates the porosity-velocity relationship is not linear. Anselmetti (2001) shows that at 40% porosity in naturally occurring carbonate systems, V_P can range from 2.5 km/s to 5 km/s. In addition to common rock properties such as porosity and fluid saturation, the pore shapes severely affect seismic velocities in carbonate rocks.

Carbonate porosity can be generated before, during, or after deposition (Scholle and Foundation, 1978). In carbonates there are many subgroups of porosities such as moldic, vuggy, intraparticle (within particles) and interparticle (between particles) as shown in Figure 5 (Bathurst, 1972; Scholle and Foundation, 1978). From rock physics point of view, the major difference of porosities is their shape.

Through many experimental and theoretical research, it has been proven that pore shapes (geometry) influence sonic velocities (Anselmetti, 2001; Cheng and Toksöz, 1979; Eberli et al., 2003; Kuster and Toksöz, 1974a; Sayers, 2008; Toksöz et al., 1976; Wang et al., 1991; Xu and Payne, 2009; Xu and White, 1995). Eberli et al. (2003) pointed out that porosity-velocity relationship is very different for rocks with different pore spaces such as micro, moldic and intercrystal pores. Laboratory experiments show that caves in carbonate rocks do not have any contribution to sonic velocity change due to their high rigidity. However, micro-pores or cracks significantly decrease sonic velocities due to their low rigidity (Wang et al., 2011). Rocks with rounded pores such as moldic and vuggy pores, generally have higher velocities than rocks with flat pores such as microcracks or penny shape pores (Xu and Payne, 2009). Most rock physics models assume spherical grains and homogeneous pore system for the rocks. The key in carbonate petrophysical modeling is to account for the pore shapes. Since pore shapes are more complex in carbonate rocks than in clastic rocks, developing an appropriate rock physics model for carbonate rocks is extremely difficult (Xu and Payne, 2009).

Beside the pore shape, as an undeniable factor in interpreting sonic velocities in carbonate, there could be some other factors such as:

1) Type of cementation. There are different types of cements in carbonates such as 1) meniscus which is only found at grain contacts, 2) isopachous, which grows along entire grains. The presence of different types of cements in the rock has different influences on stiffness of the rocks

and their sonic velocities. Thus, the type of cementation, should be considered at the time of analyzing sonic velocities (Scholle and Foundation, 1978).

2) Micrite content. High micrite content (low grain to micrite matrix ratio) typically indicates a low energy environment. These rocks are relatively very stiff and impermeable. On the other hand, lower percentage of micrite (high grain to micrite matrix ratio) which can be found in the rocks due to the higher energy of the depositional systems, or removing it from intergranular macropores by progressive leaching of the matrix, will cause increasing porosity and reducing rock stiffness. Subsequently, this will decrease sonic velocities. There is a correlation between decreasing micrite and increasing macroporosity. As microporosity within micrite does not significantly contribute to fluid flow, the permeability of the rocks increases with increasing macroporosity. It can be concluded that there should be a connection between sonic velocities and the content of the microcrystalline matrix (Vanorio and Mavko, 2011).

3) There are some isolated micropores within the rock mass and also within insitue OM (Scholle and Foundation, 1978; Slatt and O'Brien, 2011). As mentioned earlier one of the assumptions of Gassmann's equations is having well-connected pores which are fully filled with a nonviscous fluid. Although Gassmann's equations are approved and well known for considering effect of pore fluids on sonic velocities, they are not completely correct. This problem is not unique to carbonate rocks. However, it is more significant in carbonates compared to other siliciclastic rocks due to existence of vast variety of pores types in them.

CHAPTER III

METHODS

Rock physics combines empirical and theoretical relationships to connect intrinsic rock properties such as mineralogy, porosity, pore shape, pore fluid, and pore pressure, to their elastic moduli and subsequently elastic velocities (Mavko et al., 2009; Sayers, 2013). For purposes of seismic exploration, it is important to compute elastic velocities of saturated rock as a function of their porosity, ϕ. Through rock physics it can be achieved in two steps. In the first step, the elastic moduli of dry/drained rock and pore fluids are estimated separately. In the second step they are merged using a substitution method such as Gassmann's substitution (Mavko et al., 2009).

3.1 Dry/Drained Rock Moduli

3.1.1 End Member

To express dry rock moduli as a function of ϕ, first their end member values, i.e., at minimum (zero) and maximum (critical[1]) ϕ are needed to be computed. At zero porosity moduli are computed by Hill's average (Equation 2) (Mavko et al., 2009).

$$K = 0.5 \cdot [\sum_{i=1}^{m} f_i K_i + (\sum_{i=1}^{m} f_i / K_i)^{-1}], \quad G = 0.5 \cdot [\sum_{i=1}^{m} f_i G_i + (\sum_{i=1}^{m} f_i / G_i)^{-1}] \qquad 2$$

In Equation 2, m: number of minerals within solid rock; f_i, K_i and G_i are: volumetric fraction, bulk modulus and shear modulus of i^{th} mineral, respectively.

[1] Porosity at which the mineral grains starts to become suspended within the pore fluid

At critical porosity and hydrostatic pressure, elastic moduli are calculated by the Hertz-Mindlin method (Mavko et al., 2009) (Equation 3), which expresses the effective bulk and shear moduli of random sphere packing through porosity, sphere radius, normal and tangential stiffnesses, and coordination number. The average number of contacts per grain, known as coordination number, typically varies from 5 to 9 in sedimentary rocks (Mavko et al., 2009).

$$K_{HM} = \left[\frac{n^2(1-\phi_c)^2 G^2}{18\pi^2(1-\nu)^2} P\right]^{\frac{1}{3}}, \qquad G_{HM} = \frac{5-4\nu}{5(2-\nu)}\left[\frac{3n^2(1-\phi_c)^2 G^2}{2\pi^2(1-\nu)^2} P\right]^{\frac{1}{3}} \qquad 3$$

In Equation 3, n: coordination number; P: the hydrostatic pressure; G is the shear modulus of the solid phase, and ν is the Poisson's ratio of solid phase defined as:

$$\nu = 0.5\frac{K-{}^2/_3 G}{K+{}^1/_3 G} \qquad 4$$

3.1.2 Intermediate

Elastic moduli of the dry rock as a function of ϕ between the two end-member cases vary in a variety of ways. In this project, the broad categories of variations are: 1) pore-shape independent, and 2) pore shape dependent models. In the first category, as the name suggests, the elastic moduli of the rocks are just dependent on the value of ϕ and not their geometry. In the second category the shape of the pores matter.

3.1.2.1 Pore Shape Independent Models

a) Stiff and Soft Pores

The generic classification in this category is based on the behavior of pore shapes under external pressure. For example, when the material is unconsolidated, small increases in the overburden pressure may lead to rather large reductions in pore volume and increase in moduli. This may be

true for well-consolidated rocks, where the reduction in porosity is more proportional to the overburden pressure. If the pores are easily deform under stress field, the pores are referred to as "soft", otherwise they are referred to as "stiff."

The behavior of rock with "stiff" or "soft" pores can be respectively modeled using the upper and lower HS bounds, where the rock is assumed as a dense random pack of identical spherical grains at critical porosity.

The generalized elastic moduli for stiff pores for $\phi < \phi_c$ is given by:

$$\begin{cases} K_{Dry} = [\dfrac{\phi/\phi_c}{K_{HM} + \frac{4}{3}G} + \dfrac{1-\phi/\phi_c}{K + \frac{4}{3}G}]^{-1} - \dfrac{4}{3}G_{HM} \\ G_{Dry} = [\dfrac{\phi/\phi_c}{G_{HM} + Z} + \dfrac{1-\phi/\phi_c}{G + Z}]^{-1} - Z \end{cases} \quad 5$$

In Equation 5, Z is:

$$Z = \frac{G}{6}\left(\frac{9K + 8G}{K + 2G}\right) \quad 6$$

The generalized elastic moduli for soft pores for $\phi < \phi_c$ is given by:

$$\begin{cases} K_{Dry} = [\dfrac{\phi/\phi_c}{K_{HM} + \frac{4}{3}G_{HM}} + \dfrac{1-\phi/\phi_c}{K + \frac{4}{3}G_{HM}}]^{-1} - \dfrac{4}{3}G_{HM} \\ G_{Dry} = [\dfrac{\phi/\phi_c}{G_{HM} + Z} + \dfrac{1-\phi/\phi_c}{G + Z}]^{-1} - Z \end{cases} \quad 7$$

For soft pores, the effective ϕ can exceeds ϕ_c. In such a case, the generalized elastic moduli can be expressed as:

$$\begin{cases} K_{Dry} = [\dfrac{(1-\phi)/(1-\phi_c)}{K_{HM} + \frac{4}{3}G_{HM}} + \dfrac{(\phi-\phi_c)/(1-\phi_c)}{\frac{4}{3}G_{HM}}]^{-1} - \dfrac{4}{3}G_{HM} \\ G_{Dry} = [\dfrac{(1-\phi)/(1-\phi_c)}{G_{HM} + Z} + \dfrac{(\phi-\phi_c)/(1-\phi_c)}{Z}]^{-1} - Z \end{cases} \quad 8$$

In equations 7-8, Z is:

$$Z = \frac{G_{HM}}{6}\left(\frac{9K_{HM} + 8G_{HM}}{K_{HM} + 2G_{HM}}\right) \quad 9$$

b) Floating pores

In special geological cases, such as for hydrate-bearing sediments, both stiff and soft pores can simultaneously exist in the rock. For example, when hydrate fills an interconnected set of fractures, it can be viewed as forming a stiffer shell which includes the softer, host sediments. Similarly, when hydrate fills a set of disconnected fractures, it can be viewed as a stiffer inclusion. The elastic behavior of the rock can then be modeled using a combination of lower and upper HS bounds. The rock can be assumed to comprise two closed systems:

$$Components\ of\ a\ rock\ with\ fracture\ system \begin{cases} 1.\ the\ background\ matrix \\ (including\ its\ own\ pore\ spaces\ and\ fluid\ saturations) \\ 2.\ fracture\ system \\ (including\ its\ own\ fluid\ saturations) \end{cases}$$

Further, it is assumed that the two closed systems do not interact with each other. The pores within the first closed system, the background matrix, could be independently treated as stiff or soft depending on the state of their consolidation. Using either of the models, the bulk and shear moduli of the *saturated* background matrix can be estimated. The *saturated* background matrix can then be mixed with the fracture system using the lower or upper HS bound. An additional complexity in hydrate-bearing fractures is that they are also saturated partially with fluids. As a result, overall, the rock has three components:

Components of whole rock $\begin{cases} 1. \text{saturated background matrix} \\ 2. \text{hydrate within the fractures} \\ 3. \text{brine within the fractures} \end{cases}$

When the stiffest component of these cases is assumed to form the outer shell for a Hashin type assemblage, the pores are in their stiffest possible state. On the other hnad, if the softest component of these cases is assumed to form the outer shell for a Hashin type assemblage, the pores are in their softest possible state. The formulation is as follows:

$$K = \left[\sum_{i=1}^{3} \frac{f_i}{K_i + \frac{4}{3} G_{(\min/\max)}} \right]^{-1} - \frac{4}{3} G_{(\min/\max)} \quad 10$$

$$G = \left[\sum_{i=1}^{3} \frac{f_i}{G_i + Z_{(\min/\max)}} \right]^{-1} - Z_{(\min/\max)} \quad 11$$

$$Z_{(\min,\max)} = \frac{1}{6} G_{(\min/\max)} \left(\frac{9K_{(\min/\max)} + 8G_{(\min/\max)}}{K_{(\min/\max)} + 2G_{(\min/\max)}} \right) \quad 12$$

In Equations 10-12, *i* is the number of rock components. *f*, *K* and *G* present the volumetric fraction, bulk modulus, and shear modulus of each component, respectively. Subscribes ‘min’ and ‘max’ refers to minimum and maximum elastic modulus of the three above-mentioned components.

3.1.2.2 Pore Shape Dependent

Experimentally, it has been found that when pore shapes are spherical, the elastic velocities are higher compared to when they are oblate (Anselmetti et al., 1997; Eberli et al., 2003; Sayers, 2008; Xu and Payne, 2009; Zhao et al., 2011). Being able to account for the pore shapes becomes important in rocks such as carbonates. Here a set of models proposed by Kuster and Toksöz

(1974a) are being tested, mainly due to the models' flexibility in accounting for pore shapes. These models assumed that the rock is isotropic, the porosity is low and pore shapes are idealized ellipsoidal. In this model, the spherical pores present almost the same sonic velocities as the upper HS model does but it is limited to low porosities (Berryman, 1980; Kuster and Toksöz, 1974a). Bulk (K_{KT}) and shear (G_{KT}) moduli of Kuster and Toksoz model are expressed by Equations 13 and 14.

$$(K_{KT} - K_m)\frac{\left(K_m+\frac{4}{3}G_m\right)}{\left(K_{KT}+\frac{4}{3}G_m\right)} = \sum_{i=1}^{N} x_i(K_i - K_m)P^{mi} \qquad 13$$

$$(G_{KT} - G_m)\frac{\left(G_m+\frac{4}{3}\zeta_m\right)}{\left(K_{KT}+\frac{4}{3}\zeta_m\right)} = \sum_{i=1}^{N} x_i(G_i - G_m)Q^{mi} \qquad 14$$

In Equations 13 and 14, the subscript m and i represents background and pore fluid materials; The summation is over fluid types with volume concentration x_i; ζ is computed by Equation 15.

$$\zeta = \frac{\mu}{6}\frac{(9K+8G)}{(K+2G)} \qquad 15$$

In Equation 15, K and G are bulk and shear modulus of the rock at zero porosity, respectively and P^{mi} and Q^{mi} represents the effect of the i^{th} pore fluids within a background matrix, m (Table 1).

Table 1. P^{mi} and Q^{mi} for some specific pore types(Berryman, 1995)

Pore Shape	P^{mi}	Q^{i}
Sphere	$\frac{K_m+\frac{4}{3}G_m}{K_i+\frac{4}{3}G_m}$	$\frac{G_m+\zeta_m}{G_i+\zeta_m}$
Needle	$\frac{K_m+G_m+\frac{1}{3}G_i}{K_i+G_m+\frac{1}{3}G_i}$	$\frac{1}{5}\left(\frac{4G_m}{G_m+G_i}+2\frac{G_m+\gamma_m}{G_i+\gamma_m}+\frac{K_i+\frac{4}{3}G_m}{K_i+G_m+\frac{1}{3}G_m}\right)$
Penny Shape	$\frac{K_m+\frac{4}{3}G_i}{K_i+\frac{4}{3}G_i+\pi\alpha\beta_m}$	$\frac{1}{5}\left(1+\frac{8G_m}{4G_m+\pi\alpha(G_m+2\beta_m)}+2\frac{K_i+\frac{2}{3}(G_i+G_m)}{K_i+\frac{4}{3}G_i+\pi\alpha\beta_m}\right)$
$\beta=\mu\frac{(3K+G)}{(3K+4G)}$, $\gamma=\mu\frac{(3K+G)}{(3K+7G)}$, $\zeta=\frac{G}{6}\frac{(9K+8G)}{(K+2G)}$		

3.2 Fluid Moduli

The bulk modulus of fluid changes under pressure and temperature gradients which can be

computed by Batzle and Wang (1992) empirical formulas. In presence of different pore fluids within the pore spaces, the total bulk modulus of fluid (K_f) is expressed by:

$$K_f = \left[\sum_{i=1}^{n} S_i / K_i \right]^{-1} \qquad 16$$

In Equations 16, S_i and K_i represents the saturation and bulk modulus of ith fluid component.

3.3 Saturated Rock Moduli

Gassmann's substitution is a tool to compute elastic moduli of saturated rock. Although the Gassmann's substitution is independent of pore geometries, it has several underlying assumptions including 1) isotropic rock and homogenous mineral moduli, 2) no interaction between rock and fluid, which means diagenetic processes, such as cementation and dissolution, do not increase or decrease the porosity of the rocks, 3) connected pores, which cause an equilibrium pressure, a uniform distribution of the fluid within pore spaces, and 4) a closed system, which results in no fluid movement across the boundaries. Further, Gassmann's equations are generally valid in the low (seismic) frequency range, because low frequency gives enough time for relaxation of the disturbed fluid within the pores. Error in Gassmann's analytical methods is generally thought to increase at ultrasonic (logging) frequencies (Al-Khateb, 2013; Avseth et al., 2005; Berryman, 1999; Kumar et al., 2006; Mavko et al., 2009), however Røgen et al. (2005) and Adam et al. (2006) have also shown that it may not be necessarily true unless the rock has a preferential fabric. The saturated moduli is expressed as:

$$K_{Sat} = K \frac{\phi K_{Dry} - (1+\phi) K_f K_{Dry} / K + K_f}{(1-\phi) K_f + \phi K - K_f K_{Dry} / K} \quad , \quad G_{Sat} = G_{Dry} \qquad 17$$

In Equation 17, K_{Dry} and G_{Dry} are the dry rock moduli; K is the bulk modulus of the solid phase at zero porosity; and K_f is fluid modulus.

3.4 Sonic Velocities

Estimation of elastic velocities requires estimation of both elastic moduli and bulk density (ρ_b), which is expressed as:

$$\rho_b = (1-\phi)\rho_s + \phi\rho_f \quad (18)$$

In Equation 18, ϕ is porosity, ρ_s and ρ_f are respectively matrix and fluid densities. ρ_s and ρ_f are expressed by Equations 19 and 20:

$$\rho_s = \sum_{i=1}^{m} f_i \rho_i \quad (19)$$

$$\rho_f = \sum_{i=1}^{n} S_i \rho_i \quad (20)$$

Batzle and Wang (1992) empirical formulas are used to calculate fluid density under reservoir pressure and temperature.

Here, both saturated and dry rock velocities are being modeled. The saturated rock data is acquired *in-situ* in the field using well logs. The dry rock data are acquired from the outcrop samples. For their respective sets, the elastic velocities are expressed as:

$$Vp = \sqrt{\left(K_{Dry\ or\ Sat} + \frac{4}{3} G_{Dry\ or\ Sat}\right) \Big/ \rho_b} \quad (21)$$

$$Vs = \sqrt{G_{Dry\ or\ Sat} \Big/ \rho_b} \quad (22)$$

CHAPTER IV

RESULTS

In this project, applications of rock physics models in quantitative interpretation of sonic velocities are demonstrated in three unconventional reservoirs, 1) Woodford Shale from McNeff 2-28 Well, Grady County, Oklahoma, 2) gas hydrate from Krishna-Godavari Basin, and 3) Mississippian carbonate from the Blackbird 4-33, Osage County, Oklahoma. In this chapter, reasons of applying the stiff model, the combined stiff and soft model, and the Kuster and Toksoz model, respectively, to the above-mentioned reservoirs are explained. For the first two reservoirs, data have been acquired under saturated conditions. These data includes well logs such as dipole sonic, density and porosity logs. For the third reservoir, data have been acquired under dry conditions. These data include sonic velocities at ultrasonic frequencies, SEM, XRD, and bulk ϕ. Parameters such as mineralogy, porosity, and pore shapes are inputs to the rock physics models, which output the sonic velocities. To check the validity of the rock physics models, the inputs and outputs of the models are compared with the field and laboratory data.

4.1 Woodford Shale as Stiff Pore System

a) Data

The Woodford Shale under investigation is from the McNeff 2-28 well, Grady County, Oklahoma. Available logs include dipole sonic and density and neutron porosity. The depth of Woodford Shale in the McNeff 2-28 well is from 10,280ft to 10,450ft. Due to the buried depth and confining pressure, the Woodford Shale is assumed to be a stiff pore system. Application of

the stiff sand model is tested to quantitatively interpret sonic velocities obtained from the dipole sonic log.

b) Rock Physics Context

Photoelectric factor value, X-ray diffraction and gamma ray information show that quartz, calcite, and illite are the three dominant components of the Woodford Shale (Caldwell, 2011; Jarvie, 2008). Petroleum industry databases such a production data from the Oklahoma City Geological Society Library provide data that indicates gas and brine are the dominant fluids of the formation. Further, the Woodford Shale of the McNeff 2-28 well is enriched by OM. Placing the OM as part of pore fluid or rock matrix is extensively explored in this study.

c) Synthetic Model

To illustrate the effect of different individual factors such as porosity, mineralogy, and fluid saturation of the Woodford Shale on sonic velocities, a synthetic model is designed. The synthetic model is a base section with thickness of 170ft (52m, equal to the thickness of Woodford Shale in McNeff 2-28 well), 100% illite, 5% porosity (ϕ), and 100% brine saturated (Figure 6). Figure 6a presents the effect of pressure on sonic velocities. The applied temperature for measuring elastic moduli of fluid is 76 ℃, which is taken from the McNeff 2-28 Well. Figure 6b illustrates the effect of changing, ϕ, mineralogy, and fluid saturation on sonic velocities. Separately, illite is replaced with calcite and quartz to examine the effect of increasing Calcite and Quartz on sonic velocities. Similarly, effect of increasing gas is shown by replacing brine with gas. Unlike other reservoirs, in shale, OM plays a vital role in deciding its productivity. To find the effect of increasing OM on sonic velocities, one time the OM is assumed to be a ‘mineral’ and another time a ‘fluid’. In the case of considering OM as a mineral, OM is replaced with illite (matrix component). And in the case of considering OM as a fluid, OM is replaced with brine (fluid component).

Figure 6b presents that a) increasing ϕ decreases sonic velocities, b) replacing illite with quartz and calcite increases sonic velocities, c) increasing OM as a fluid or a mineral decreases sonic velocities. However the magnitude of the decrease in sonic velocities in the case of considering OM as a mineral is almost twice the case that OM is considered as a fluid, d) increasing gas saturation decreases Vp and slightly increase Vs, which follow the Eq.17 and 18, where shear modulus of saturated rock remain constant and bulk density decreases. Highest sensitivity of Vp to gas saturation occurs when gas saturation changes from 0 to 10%. Figure 6a also suggests that effect of pressure on sonic velocities is fairly insignificant in comparison with other above-mentioned factors. Thus a constant pressure of 61.36 MPa is assumed for the McNeff 2-28 well.

d) Real Data

The first step require to use the well log data from the Woodford Shale in McNeff 2-28 well, was to construct a cross-plot using Vp and Vs. The presented trend for Vp vs. Vs is the ease of comparison between sonic velocities obtained from the log and computed from the stiff-sand model. Obtaining seismic velocities at a log interval (0.5 ft) is almost impossible. For the Woodford Shale in the McNeff 2-28 well, buried at > 10,000ft and with thickness of 170ft (52m), a linear Vp and Vs trend is expected from conventional seismic processing methods. A linear fit to the well log data (solid red lines; Figure 7a) can represent the obtained Vp-Vs cross plot from seismic survey. Here the mentioned fit is called the "surface seismic trend."

It is assumed that seismic data is available and a Vp-Vs trend, similar to surface seismic trend, can be obtained from the seismic data. Therefore, introduced surface seismic trend is used instead of log data in this case study to reconstruct ϕ and composition depth profiles of the Woodford using a rock physics model. Note that, due to 'random noises' and 'seismic processing simplifications,' computed 'surface seismic trend' is associated with large standard deviation. On

the other words, predicting Vp-Vs trend of seismic data, without any standard deviation, using well log data is impossible. It is assumed that the standard deviations of the surface seismic trend for the McNeff 2-28 is at least the same as the standard deviation in the log data. In Figure 7b, the surface seismic trend is presented in the Vp-Vs space, and with a solid white line. The width of solid line is proportional to Vp and Vs standard deviations.

To generate a unique Vp and Vs depth profile from the stiff-sand model, porosity, composition, fluid saturation, reservoirs pressure, etc. can be combined in multiple ways. Now the question is "can a unique ϕ and composition be inferred from collocated Vp and Vs depth profiles?" Through trial-and-error forward modeling and by changing applied ϕ and composition in the model, it is understood that the surface seismic trend can be fitted to the level of its variance for two end-member compositional scenarios, with OM located in matrix and OM located in pore-fluid. Despite the fact that both scenarios generated a perfect match of surface seismic trend and sonic velocities obtained from the rock physics model, the inputs of the model (ϕ, composition) are different for different scenarios (Table 2). It is necessary to determine which end member scenario is more realistic.

Table 2. Table 3. Stiff-sand parameter depth profiles

	OM in matrix		OM in pore fluid	
	W. Top	W. Base	W. Top	W. Base
f_Q (%)	84±5	60±5	76±5	20±5
ϕ (%)	15±0.1	14±0.1	15±0.1	17±0.1
f_O (%)	0.0±0.01	2.5±0.01	1.5±0.01	4.1±0.01
f_C (%)	0.0	0.0	1.5±0.5	3.9±0.5
S_G (%)	34±5	30±5	16±5	35±5

By considering OM within the matrix, a perfect (almost zero standard deviation) match of the surface seismic trend and outcome of rock physics model is achieved by the following inputs: from Woodford top to base, quartz fraction decreases from 84% to 60%; OM increases from 0% to 2.5%; ϕ decreases from 15% to 14%; and gas saturation decreased from 34% to 30% (Table 2). If OM is assumed as a pore fluid, following inputs are used: from the Woodford top to base

quartz fraction decreases from 76% to 20%; ϕ increases from 14% to 17%; OM saturation within the pore spaces increases from 10% to 40% (equivalent to 1.4-6.8% of total volume of the rock); gas saturation increases from 16% to 34%; calcite increases from 1.5% to 4% (Table 2).

The quartz fraction depth profile in both scenarios imply that upper section of the Woodford Shale in the McNeff 2-28 has more quartz than its base which is confirmed with general knowledge about the study area (Harris et al., 2010 and Watson, 2008). Core analyses from Campbell 1-34 well which is located ~ 1 km southeast of McNeff 2-28 well, show high quartz content in the upper part of the Woodford Shale (Portas and Slatt, 2010).

The ϕ and ρ of the composition as inputs of the model are compared with ϕ and ρ of log data. The ϕ is provided by density-porosity ($\rho\phi$) and neutron-porosity (nϕ) logs. In both scenarios, the input ϕ profile is closer to $\rho\phi$ log than nϕ log (Fig. 6d). By increasing depth, separation between nϕ and $\rho\phi$ increases. This separation can be due to, a combination of increasing illite fraction and/or decreasing gas saturation (Asquith and Krygowski, 2004), which is suggested by the first scenario (Table 2).

If OM is part of matrix, the bulk density increases from 2.41 g/cm3 at the Woodford top to 2.47 g/cm3 at the Woodford base. Considering OM as a fluid, causes increasing $\rho\phi$ from 2.37 g/cm3 toward the Woodford top to 2.41 g/cm3 toward the Woodford base. As Figure 7c depicts, the input ρ in the second scenario has an overall better match to the ρ log. Thus, the second scenario is more realistic. Effective ϕ is subtraction of immobile fluid (OM) from total ϕ, (total ϕ-OM). In the other word, the portion of ϕ which is occupied by mobile components such as gas and brine is called effective ϕ. Although predicting effective ϕ in the absence of core is difficult, increasing the illite construction from the top to the base of the Woodford Shale results in decreasing effective ϕ (Morris and Shepperd, 1982). It is important to note that the effective ϕ is up to 40% less than the total ϕ.

4.2 Hydrate Bearing Fracture as Combined Stiff and Soft Pore System

a) Data

The gas hydrates under investigation are from the NGHP-01-10, Krishna-Godavari Basin, India (east coast). Available logs include dipole sonic, $\rho\phi$ and core measurements. The depth of gas hydrates in the NGHP-01-10 well is from ~26 mbsf (meters below sea floor) to ~156 mbsf. The effective pressure of the formation is around 1.2 MPa due to ~1000m of water depth. Due to the saturation of gas hydrate within cracks through almost the entire length of the hydrate stability zone (HSZ) (Collett et al. 2008), the studied gas hydrates are assumed to be a floating pore system (combination of soft and stiff pores). Application of floating pore model is tested to quantitatively interpret sonic velocities obtained from dipole sonic log.

b) Rock Physics Context

Core analyses, included x-ray and gamma ray log information show that clay and quartz, are two dominant components of the gas hydrate in NGHP-01-10. Core measurements from the NGHP-01-10 well and observations from other wells (from the same basin) such as NGHP-10B-18Y, indicate that pore spaces of the formation are mainly filled by brine, and around 20 to 25% of ϕ is filled by gas hydrate (Collett et al., 2008).

c) Synthetic Model

To illustrate the behavior of the floating pore model in predicting sonic velocities, a synthetic model is designed. The synthetic model has 80% clay and 20% quartz and the total ϕ (ϕ_t) is 55%. The rock is filled with 100% brine and it is replaced with 0 to 40% (out of ϕ_t) gas hydrate. The floating pore model, provides upper and lower bounds, Figure 8. It is often applicable and adequate to represent the elastic moduli of a mixed mineralogy by either one of the HS bounds (upper or lower) or their average, $(M^{HS+}+M^{HS-})/2$. This is applicable due to the fact that many

models (e.g. Gassmann, Kuster-Toksoz, etc.) assume a homogenous mineral modulus (Mavko et al., 2009). As explained, upper and lower bounds of the floating pore model are modification of HS bounds. Thus, in Figure 8, the average of upper and lower bounds of the floating pore model is presented. In addition to the floating pore model, Figure 8 depicts the results of upper and lower HS and soft sand model. Since the data is from shallow depth, the sediments are loose and unconsolidated. Thus, stiff sand model is not applicable for the gas hydrate study. In HS and soft sand model, the gas hydrate is preserved within the void spaces of the rock. Using these models, distinguishing pore spaces and fracture systems is not possible. However, in floating pore model, ϕ_t has two parts 1) matrix ϕ (ϕ_M), 2) fracture ϕ (ϕ_f), respectively, 33% and 22% in this synthetic model. Although gas hydrate can be preserved within both mentioned porosities (ϕ_M and ϕ_f), in this case study it is assumed that gas hydrate just fills ϕ_f (not ϕ_M). As shown in the Figure 8, both HS and floating pore models release maximum and minimum possible sonic velocities at each specific ϕ. Results of the floating pore model is more confined compared to the HS model. For example, at hydrate saturation equal to 20%, predicted Vp from HS and floating pore model are in the range of 1.6 - 3.1 km/s and 1.7 - 2 km/s, respectively. This example confirms that the range of predicted velocity for the fracture model (2-1.7= .3 km/s) is less than the range for the HS model (3.1-1.6=1.5 km/s). It is noticeable that though the soft pore model and the average trend of the floating pore model present similar sonic velocities at each ϕ value, their interpretations about the location of gas hydrate preservation in the void spaces of the rocks are different.

d) Real Data

To use the well log data from NGHP-01-10, each individual log is presented vs. depth. By changing fraction of ϕ_M and ϕ_f out of ϕ_t the velocities are predicted through the formation (top to bottom of the formation) and compared with obtained sonic velocities from dipole sonic log. If there exists a match between predicted and obtained sonic velocities, the validity of the model is

checked by comparing applied bulk densities, dry bulk densities and porosities as inputs of the model and acquired from core analysis.

The model outputs, sonic velocities, depend on multiple inputs including saturation of hydrate within background matrix (S_{hBM}) and in fractures (S_{hf}). In the floating pore model, ϕ_t remains fairly consistent along the length of the log. Further, core description and seismic profiles show that ϕ_f does not change drastically along the length of the core (Jaiswal et al., 2012a). Here, it is assumed that:

ϕ_f =X% ϕ_M (Notice: $\phi_t = \phi_f + \phi_M$)

X presents the proportion of ϕ_f to ϕ_M. Through trial-and-error modeling, it is understood that the best match between predicted sonic velocities using floating pore model and well log data is achieved at X=50%, $S_{hBM} = 10\%\phi_M$, $S_{hf} = 80\%\phi_f$. The total hydrate saturation within the rock is computed by:

$S_{ht} = S_{hBM}\ \phi_M + S_{hf}\ \phi_f$

For example, if $\phi_t = 60\%$, then: $\phi_M = 40\%$, $\phi_f = 20\%$, $S_{hBM} = 10\% \times 40\% = 4\%$, $S_{hf} = 80\% \times 20\% = 16\%$, and $S_{ht} = 4\% + 16\% = 20\%$. Figure 9 depicts the results of the model and Figure 10 shows the comparison of applied ρ and ϕ with the data from cores.

4. 3 Mississippian Carbonate as a Pore Shape Dependent System

a) Data

The Mississippian carbonate under investigation is from Blackbird 4-33 well, Osage County, Oklahoma. Available data are core measurements such as sonic velocities, porosity, thin-section, SEM, and XRD. Due to variant pore types within the carbonate rocks and their effect on controlling sonic velocities, carbonates are categorized as a pore shape dependent system out of

explained rock physics systems. Application of Kuster and Toksöz model as a pore shape dependent system is tested to interpret sonic velocities (Kuster and Toksöz, 1974a, b).

b) Rock Physics Context

XRD analyses and thin section studies show that calcite and quartz, are two dominant components of the Mississippian carbonate in the Orion core. The core sample was dried and the pores filled by air. The pore shapes vary from nearly spherical to highly elongate. The porosity value varied between 1 and 6 %.

c) Synthetic Model

To illustrate the behavior of Kuster and Toksöz (1974) model in predicting sonic velocities, a synthetic model is designed. The synthetic model has 80% calcite and 20% dolomite and ϕ varies from 0 to 20%. The rock is filled with 100% air. The Kuster and Toksöz model, provides sonic velocities of variant pore shapes such as spherical pores, needle shape pores, and penny shape pores with different α values of 0.15, 0.1, and 0.07 (Figure 11).

As it is depicted, at the same porosity, the sonic velocity of rock is higher for spherical pores compared to ellipsoid pores. For example, at ϕ of 15% the Vp varies between 3.5 and 6.3 km/s, which respectively correspond to a penny shaped pore (α=0.07) (3.5 km/s) and a spherical pore (6.3 km/s).

d) Real Data

All sonic velocities obtained from core data are shown versus ϕ in the Figure 12. As depicted here, the sonic velocities are scattered. The composition of each sample is found using XRD analyses. Using composition of the rock sample, sonic velocities are predicted from 0 to 6% ϕ for different pore shapes with different α value. If there exists a match between predicted and

obtained sonic velocities, the validity of the model is checked by comparing applied pore shape in the model and observed ones in thin-section (Figure 13).

CHAPTER V

DISCUSSION

Seismic methods are the most popular non-intrusive remote sensing tool for imaging the subsurface. They provide data for physical property maps such as elastic velocities and densities. These maps can be interpreted for delineating structures and identifying potential reservoirs. This interpretation is still qualitative in nature. Rock physics models help in quantifying the interpretation, which implies finding a relation between the physical properties maps and rock properties such as porosity and composition under *in situ* condition (i.e. pore pressure and fluid saturation). Rock physics models successfully work for conventional reservoirs, but they have not been fully explored in unconventional settings. In this thesis, a few standard rock physics models have been tested in three unconventional reservoirs, shale, gas hydrate and carbonates. Their applicability is discussed below.

The stiff sand model was applied to relate the elastic properties and rock properties of the Woodford Shale in the McNeff 2-28 well. The stiff sand model is for isotropic medium. However, shales are almost always anisotropic due to the wave propagation direction and bedding alignments (Lucier, 2010). This inconsistency can be reconciled in two ways. First, it is possible that the high quartz content in the upper section of the Woodford Shale makes the Woodford more isotropic. Second, the behavior of sonic velocities at the log and seismic scale could be different. Further, the stiff sand model predictions are within an error bar of 5%, which may include effects such as dissolution and precipitation of minerals, as well as counteraction of anisotropy by random cracks (Aplin and Macquaker, 2011; Fertl and Chilingarian, 1990). Even if

the a typical anisotropic model, such as Bandyopadhyay (2009) or Vernik and Liu (1997), were applied these effects may not have been accounted for. Therefore, applying an isotropic model such as stiff sand model, can be reasonable with non-zero standard deviation. Storvoll and Brevik (2008) found that in presence of huge standard deviation, even empirical relations can work.

Speculation on the nature of gas (adsorbed versus free or wet versus dry) is not possible with this modeling. In shale, significant amounts of gas can exist in the TOC as an adsorbed phase (Holmes et al., 2011). In this case study, the TOC has been modeled as part of matrix and gas as a part of pore fluid. Gas in the adsorbed phase will not only change the effective shear moduli of the TOC, it will also create capillary effects. There is a lack of rock physics models which sufficiently address this aspect. Lewis et al. (2004) shows that at pressures higher that ~10 MPa, such as in the McNeff 2-28 well, gas may be present dominantly in free phase. The fluid flow within the Woodford shale should be unrestricted to be able to use stiff sand model. This is due to limitations of Gassmann's equations which are used in stiff sand model. As gas permeability is higher than that of the liquids (e.g, Tanikawa and Shimamoto (2006)), it is likely that stiff sand model is better suited for gas shale than oil shale.

Application of the stiff sand model to the Woodford Shale does not attempt to convey that the Woodford can be compared to a clean sandstone. The aim is to say that rock properties of the Woodford Shale is predictable using the stiff sand model within acceptable error. This model can be applicable in other shale formations, if their reservoir conditions are similar to the Woodford Shale in the McNeff 2-28 well. Reservoir conditions here mean gas bearing, highly compacted (lithified) and high quartz content.

The second, floating model, as applied in this paper, is a combination of two isotropic models (soft/stiff pore and HS models) and therefore it is only suitable for an isotropic system. However, it is applied in this thesis to model the effects of fractures in unconsolidated sediments. As in the

previous case study, it does not imply that a system will stay isotropic in presence of fractures, but rather that in this system the fractures could be random, It is also notable that in the study area, a reasonable velocity estimate has been obtained using isotropic assumptions (Jaiswal et al., 2012b; Riedel et al., 2011). Further, the floating model can be easily extended into an anisotropic domain by applying the introduced methodology by Bandyopadhyay (2009).

In fine grained sediments, cracks are zones of higher permeability that can provide opportunities for focused-fluid flow. Higher permeability fault planes can eventually become hydrate saturated in fine grained sediments through diffusion (Bhatnagar et al., 2007). Daigle and Dugan (2010a) show that hydrate saturated formations can also create and saturate cracks through occlusion. The well NGHP-01-10 was drilled close to the crest of an anticline where gas hydrate distribution shows fault control (Jaiswal et al., 2012b). Therefore in the study area, faults due to sediment failure are expected. However, tectonic-driven cracks are generally expected to be oriented perpendicular to the extensional stress rather than being random. Hydrate distribution is also permeability driven, which can be somewhat random in fine-grained media. Randomness of cracks could be a result of hydrate occlusion, which is similar to inferences by Rees *et al.* (2011) using micro-CT scanning.

The floating model can have a wider application, particularly in rocks that are cemented. A cemented rock can be viewed as a two component system – 1) background matrix, and 2) cement. For example, in the case of carbonate rocks, the cements include meniscus (cementation filling grain contacts exemplified by micritic bridging cement) and isopachous (cement grows along entire grains as in the case of acicular cement). The meniscus and isopachous, are respectively similar to “holding hydrate filled fractures by background matrix” and “holding background matrix by hydrate filled fractures” which then can be formulated by HS- and HS+. In this case, cement should be consolidated. Otherwise the meniscus cement is always stiffer than isopachous within loose sediments when the cement is not firm enough (Eberli et al., 2003). Here the main

objective is to investigate the effects of cement types within carbonate rocks that may object elastic properties of the rock and cause variation in elastic moduli and subsequent sonic velocities. Results from laboratory measurements (such as porosity from porosimeter and composition from XRD), well log and seismic data will be used to validate and examine the application of the model.

The third, Kuster and Toksöz model, provides sonic velocities of the rock by considering its pore shapes. Both pore size and shapes vary considerably within a carbonate rock. For a dry sample, this model provided very encouraging results. However, this model remains to be the most poorly understood and with many potential pitfalls. First, is accounting for cement. Kuster's model assumes that cements are part of uniform mineralogy. This cannot be reconciled with other models that place cement (more appropriately) at grain contact locations and show a very non-linear relation between elastic velocities and cement concentration (Dvorkin et al., 1999; Dvorkin et al., 1994; Elata and Dvorkin, 1996). For example, in case of having dolomite or quartz cement in a limestone, the model considers the cement as a mineralogy which is mixed with the host rock (limestone). Therefore the model will not give an appropriate answer based on the properties of the cement. Second, this model also does not account for intrinsic porosity in OM or clay (Mavko et al., 2009; Xu and Payne, 2009). The Kuster and Toksöz model is a good fit for dry solid rocks. To apply this model to well logs, a fluid substitution mechanism, such as the Gassmann's method has to be applied. However, based on the previous explanation in Sec. 2.4, applying Gassmann's equations will not be completely correct due to the presence of isololated pore systems in carbonates. In addition, the model does not consider grain to micrite ratio and its effect on changing porosity, permeability, stiffness, and subsequent sonic velocities. In the Kuster and Toksöz model, porosity means void spaces. However the void spaces can either be pore spaces or fracture. The model cannot distinguish pore spaces from fractures. In general, aspect ratio of most fractures are less than pores. However, this does not mean all pores have higher aspect ratio than

fractures. Finally, different pores with different aspect ratios can be found in a rock. For example, the rock can have 20% spherical pores, 80% penny shape pores. The Kuster and Toksöz model does not account for the presence of different pore spaces in a rock.

Despite their under-explored and poorly understood dependencies, rock physics applications are vital. Application of appropriate rock physics models to their respective geological scenarios allows for interpretation of seismic velocities in terms of porosity and composition. Developing a rock physics model enables an examination of various what-if scenarios by consistently changing the inputs, computing the respective elastic properties, and, finally, generating synthetic-seismic traces. This approach may help create a field guide to real-seismic-data interpretation for sweet spots, particularly in unconventional systems.

CHAPTER VI

CONCLUSIONS

This thesis demonstrates that generic rock physics models that were developed for conventional siliciclastic systems can be used for predicting elastic properties in unconventional reservoirs under restricted reservoir conditions, which include a lack of anisotropy and well developed pore-connectivity. The choice of the rock physics model to use for respective unconventional systems, depends on mechanistic make-up of the unconventional system being targeted in terms of their grain geometries, consolidation, and pore shape. In this thesis, HS bounds for grain mixing and the Gassmann method for fluid substitution satisfactorily replicated the elastic velocities under saturated conditions in both Woodford Shale and gas hydrate reservoirs. On the other hand, for carbonate rocks with non-spherical pores, Kuster and Toksoz model can predict the elastic velocities of the dry rocks, but not saturated rocks. However, the Kuster and Toksoz model needs to be modified to predict sonic velocities of subsurface carbonates. In future, applying the rock physics models to unconventional systems allows for interpretation of seismic velocities in terms of porosity and composition. Developing a rock physics model for the shale, hydrate and carbonates in general enables an examination of various what-if scenarios by consistently changing the inputs, computing the respective elastic properties, and, finally, generating synthetic seismic traces. This approach may help create a field guide to real-seismic-data interpretation for sweet spots.

REFERENCES

Adam, L., Batzle, M., and Brevik, I., 2006, Gassmann's fluid substitution and shear modulus variability in carbonates at laboratory seismic and ultrasonic frequencies: Geophysics, v. 71, no. 6, p. F173-F183.

Al-Khateb, N., A look into Gassmann's Equation, Integration, geoConvention, *in* Proceedings geoConvention, Calgary, Canada, 2013, p. 1-6.

Anselmetti, F. S., 2001, Sonic velocity in carbonates—A combined product of depositional lithology and diagenetic alterations.

Anselmetti, F. S., von Salis, G. A., Cunningham, K. J., and Eberli, G. P., 1997, Acoustic properties of Neogene carbonates and siliciclastics from the subsurface of the Florida Keys: implications for seismic reflectivity: Marine Geology, v. 144, no. 1, p. 9-31.

Aplin, A. C., and Macquaker, J. H., 2011, Mudstone diversity: Origin and implications for source, seal, and reservoir properties in petroleum systems: AAPG bulletin, v. 95, no. 12, p. 2031-2059.

Avseth, P., Mukerji, T., and Mavko, G., 2005, Quantitative seismic interpretation: Applying rock physics tools to reduce interpretation risk, Cambridge University Press.

Bahorich, M., and Farmer, S., 1995, 3-D seismic discontinuity for faults and stratigraphic features: The coherence cube: The leading edge, v. 14, no. 10, p. 1053-1058.

Bandyopadhyay, K., 2009, Seismic anisotropy: Geological causes and its implications to reservoir geophysics, Stanford University.

Barber, R., and Marfurt, K., 2010, Challenges in mapping seismically invisible Red Fork channels, Anadarko Basin, Oklahoma.

Bathellier, E., Downton, J., and Sena, A., Optimizing CSG development: Quantitative estimation of lithological and geomechanical reservoir quality parameters from seismic data: ASEG Extended Abstracts, v. 2012, no. 1, p. 1-4.

Bathurst, R. G., 1972, Carbonate sediments and their diagenesis, Elsevier.

Batzle, M., and Wang, Z., 1992, Seismic properties of pore fluids: Geophysics, v. 57, no. 11, p. 1396-1408.

Berryman, J. G., 1980, Long-wavelength propagation in composite elastic media II. Ellipsoidal inclusions: The Journal of the Acoustical Society of America, v. 68, no. 6, p. 1820-1831.

-, 1995, Mixture theories for rock properties: Rock physics & phase relations: A handbook of physical constants, p. 205-228.
-, 1999, Origin of Gassmann's equations: Geophysics, v. 64, no. 5, p. 1627-1629.
Bhatnagar, G., Chapman, W. G., Dickens, G. R., Dugan, B., and Hirasaki, G. J., 2007, Generalization of gas hydrate distribution and saturation in marine sediments by scaling of thermodynamic and transport processes: American Journal of Science, v. 307, p. 861-900.
Biot, M. A., 1955, Theory of elasticity and consolidation for a porous anisotropic solid: Journal of Applied Physics, v. 26, no. 2, p. 182-185.
Bohrmann, G., Greinert, J., Suess, E., and Torres, M., 1998, Authigenic carbonates from the Cascadia subduction zone and their relation to gas hydrate stability: Geology, v. 26, no. 7, p. 647-650.
Caldwell, C., 2012, Rock types and lithostratigraphy of the Devonian Woodford Shale, Anadarko Basin,

west-central Oklahoma, AAPG Annual Convention and Exhibition: Long Beach, California, AAPG.
Caldwell, C. D., Lithostratigraphy of the Woodford Shale, Anadarko Basin, West-Central Oklahoma, *in* Proceedings Oklahoma Geological Survey Shales Moving Forward Workshop, July2011, Volume 21, p. 2011.
Cardona, R., Batzle, M., and Davis, T. L., Shear wave velocity dependence on fluid saturation, *in* Proceedings 71st SEG Meeting, San Antonio, Texas, USA, Expanded Abstracts2001, p. 1712-1715.
CGG-Website, 2014, CGG: Unconventional Resources, Volume 2014: Passion for Geoscience, CGG Company
Cheng, C. H., and Toksöz, M. N., 1979, Inversion of seismic velocities for the pore aspect ratio spectrum of a rock: Journal of Geophysical Research: Solid Earth (1978–2012), v. 84, no. B13, p. 7533-7543.
Choquette, P. W., and Pray, L. C., 1970, Geologic nomenclature and classification of porosity in sedimentary carbonates: AAPG bulletin, v. 54, no. 2, p. 207-250.
Cipolla, C. L., Fitzpatrick, T., Williams, M. J., and Ganguly, U. K., Seismic-to-simulation for unconventional reservoir development, *in* Proceedings SPE Reservoir Characterisation and Simulation Conference and Exhibition2011, Society of Petroleum Engineers.
Collett, T. S., Riedel, M., Cochran, J. R., Boswell, R., Kumar, P., and Sathe, A., 2008, Indian continental margin gas hydrate prospects: results of the Indian National Gas Hydrate Program (NGHP) expedition 01.
Cook, A. E., Anderson, B. I., Malinverno, A., Mrozewski, S., and Goldberg, D. S., 2010, Electrical anisotropy due to gas hydrate-filled fractures: Geophysics, v. 75, no. 6, p. F173-F185.
Curtis, M. E., Cardott, B. J., Sondergeld, C. H., and Rai, C. S., 2012a, Development of organic porosity in the Woodford Shale with increasing thermal maturity: International Journal of Coal Geology, v. 103, p. 26-31.
Curtis, M. E., Sondergeld, C. H., Ambrose, R. J., and Rai, C. S., 2012b, Microstructural investigation of gas shales in two and three dimensions using nanometer-scale resolution imaging: AAPG bulletin, v. 96, no. 4, p. 665-677.

Dahl, J., Moldowan, J. M., Walls, J., Nur, A., and DeVito, J., 2012, Creation of Porosity in Tight Shales during Organic Matter Maturation, AAPG Annual Convention and Exhibition, Volume Search and Discovery Article #40979: Long Beach, California, USA.

Dai, J., Xu, H., Snyder, F., and Dutta, N., 2004, Detection and estimation of gas hydrates using rock physics and seismic inversion: Examples from the northern deepwater Gulf of Mexico: The Leading Edge, v. 23, no. 1, p. 60-66.

Daigle, H., and Dugan, B., 2010a, Effects of multiphase methane supply on hydrate accumulation and fracture generation: Geophysical Research Letters, v. 37.

Daigle, H., and Dugan, B., 2010b, Origin and evolution of fracture-hosted methane hydrate deposits: Journal of Geophysical Research: Solid Earth (1978–2012), v. 115, no. B11.

Dowdell, B. L., Roy, A., and Marfurt, K. J., 2012, An integrated study of a Mississippian tripolitic chert reservoir–Osage County, Oklahoma, USA, SEG Technical Program Expanded Abstracts 2012, Society of Exploration Geophysicists, p. 1-5.

Dvorkin, J., Berryman, J., and Nur, A., 1999, Elastic moduli of cemented sphere packs: Mechanics of materials, v. 31, no. 7, p. 461-469.

Dvorkin, J., and Nur, A., 1996, Elasticity of high-porosity sandstones: Theory for two North Sea data sets: Geophysics, v. 61, no. 5, p. 1363-1370.

-, 1998, Time-average equation revisited: Geophysics, v. 63, no. 2, p. 460-464.

Dvorkin, J., Nur, A., and Yin, H., 1994, Effective properties of cemented granular materials: Mechanics of materials, v. 18, no. 4, p. 351-366.

Eberhart-Phillips, D., Han, D.-H., and Zoback, M. D., 1989, Empirical relationships among seismic velocity, effective pressure, porosity, and clay content in sandstone: Geophysics, v. 54, no. 1, p. 82-89.

Eberli, G. P., Baechle, G. T., Anselmetti, F. S., and Incze, M. L., 2003, Factors controlling elastic properties in carbonate sediments and rocks: The Leading Edge, v. 22, no. 7, p. 654-660.

Ebrahimi, P., and Jaiswal, P., 2014, Enhancement of sub-basalt stratigraphy of Fareo-Shetland Basin using directional-filter, SEG International Exposition and 84th Annual Meeting, Volume SEG Technical Program Expanded Abstracts 2014: Denver, Society of Exploration Geophysicists, p. 1570-1574.

Ebrahimi, P., Oskouei, M., Keshavarz, N., and Ismaeili, S., 2014, Seismic Attributes Integration by GIS for Fracture Detection: Energy Sources, Part A: Recovery, Utilization, and Environmental Effects, v. 36, no. 9, p. 974-981.

Elata, D., and Dvorkin, J., 1996, Pressure sensitivity of cemented granular materials: Mechanics of materials, v. 23, no. 2, p. 147-154.

Ernstson, K., Schüssler, U., Claudin, F., and Hiltl4, M., 2011, Unusual melt rocks from meteorite impact: ERNSTSON CLAUDIN IMPACT STRUCTURES – METEORITE CRATERS.

Fertl, W. H., and Chilingarian, G. V., 1990, Hydrocarbon resource evaluation in the Woodford shale using well logs: Journal of Petroleum Science and Engineering, v. 4, no. 4, p. 347-357.

Fossen, H., 2010, Structural geology, Cambridge University Press.

Gassmann, F., 1951, Über die elastizität poröser medien: Vierteljahrss-chrift der Naturforschenden Gesellschaft in Zurich 96, 1-23: Paper translation at http://sepwww. stanford. edu/sep/berryman/PS/gassmann. pdf.
Gercek, H., 2007, Poisson's ratio values for rocks: International Journal of Rock Mechanics and Mining Sciences, v. 44, no. 1, p. 1-13.
Ghosh, R., Sain, K., and Ojha, M., 2010, Effective medium modeling of gas hydrate-filled fractures using the sonic log in the Krishna-Godavari basin, offshore eastern India: Journal of Geophysical Research-Solid Earth, v. 115.
Goodway, B., Perez, M., Varsek, J., and Abaco, C., 2010, Seismic petrophysics and isotropic-anisotropic AVO methods for unconventional gas exploration: The Leading Edge, v. 29, no. 12, p. 1500-1508.
Gordon, D., 2012, Understanding unconventional oil, Carnegie Endowment for International Peace.
Grainger, P., 1984, The classification of mudrocks for engineering purposes: Quarterly Journal of Engineering Geology and Hydrogeology, v. 17, no. 4, p. 381-387.
Hamdi, F., and Smith, D. T., 1982, The influence of permeability on compressional wave velocity in marine sediments: Geophysical prospecting, v. 30, no. 5, p. 622-640.
Handwerger, D. A., Keller, J., and Vaughn, K., Improved petrophysical core measurements on tight shale reservoirs using retort and crushed samples, *in* Proceedings SPE Annual Technical Conference and Exhibition2011, Society of Petroleum Engineers.
Helgerud, M., Dvorkin, J., Nur, A., Sakai, A., and Collett, T., 1999, Elastic-wave velocity in marine sediments with gas hydrates: Effective medium modeling: Geophysical Research Letters, v. 26, no. 13, p. 2021-2024.
Holmes, M., Holmes, D., and Holmes, A., 2011, A petrophysical model to estimate free gas in organic shales: AAPG Search and Discovery, v. July 2011, no. Artilcle #40781.
Hutchinson, D. R., Shelander, D., Dai, J., McConnel, D., Shedd, W., Frye, M., Ruppel, C., Boswell, R., Jones, E., and Collett, T. S., 2008, Site selection for DOE/JIP gas hydrate drilling in the northern Gulf of Mexico.
Jaiswal, P., Dewangan, P., Ramprasad, T., and Zelt, C., 2012a, Seismic characterization of hydrates in faulted, fine-grained sediments of Krishna-Godavari basin: Unified imaging: Journal of Geophysical Research: Solid Earth (1978–2012), v. 117, no. B4.
Jaiswal, P., Dewangan, P., Ramprasad, T., and Zelt, C. A., 2012b, Seismic characterization of hydrates in faulted, fine-grained sediments of Krishna-Godavari Basin: Full waveform inversion: Journal of Geophysical Research: Solid Earth, v. 117, no. B10, p. B10305.
Jaiswal, P., Varacchi, B., Ebrahimi, P., Dvorkin, J., and Puckette, J., 2014, Can seismic velocities predict sweet spots in the Woodford Shale? A case study from McNeff 2–28 Well, Grady County, Oklahoma: Journal of Applied Geophysics, v. 104, p. 26-34.
Jakobsen, M., Johansen, T., and Ruud, B., 2001, Modeled velocity and reflectivity properties of anisotropic hydrated sediments: Journal of Computational Acoustics, v. 9, no. 04, p. 1507-1522.

Jarvie, D., 2008, Geochemical Characteristics of Devonian Woodford Shale: Worldwide Geochemistry, LLC.

Jarvie, D. M., 2012, Shale resource systems for oil and gas: Part 2—Shale-oil resource systems.

Josh, M., Esteban, L., Delle Piane, C., Sarout, J., Dewhurst, D., and Clennell, M., 2012, Laboratory characterisation of shale properties: Journal of Petroleum Science and Engineering, v. 88, p. 107-124.

Kida, M., Suzuki, K., Kawamura, T., Oyama, H., Nagao, J., Ebinuma, T., Narita, H., Suzuki, H., Sakagami, H., and Takahashi, N., 2009, Characteristics of natural gas hydrates occurring in pore-spaces of marine sediments collected from the eastern Nankai Trough, off Japan: Energy & Fuels, v. 23, no. 11, p. 5580-5586.

Kleineidam, S., Rügner, H., Ligouis, B., and Grathwohl, P., 1999, Organic matter facies and equilibrium sorption of phenanthrene: Environmental Science & Technology, v. 33, no. 10, p. 1637-1644.

Koesoemadinata, A., El-Kaseeh, G., Banik, N., Dai, J., Egan, M., Gonzalez, A., and Tamulonis, K., Seismic reservoir characterization in Marcellus shale, *in* Proceedings 81st SEG Annual Meeting2011.

Korenaga, J., Holbrook, W., Singh, S., and Minshull, T., 1997, Natural gas hydrates on the southeast US margin: Constraints from full waveform and travel time inversions of wide-angle seismic data: Journal of Geophysical Research: Solid Earth (1978–2012), v. 102, no. B7, p. 15345-15365.

Kuila, U., and Prasad, M., 2013, Specific surface area and pore-size distribution in clays and shales: Geophysical Prospecting, v. 61, no. 2, p. 341-362.

Kumar, D., Hampson, D. P., Russell, B. H., Bankhead, B., Bland, S., Griffiths, P., Hodge, D., Ravaglia, A., Raghunath, H., and Abraham, J., 2006, A tutorial on Gassmann fluid substitution: formulation, algorithm and Matlab code: matrix, v. 2, p. 1.

Kuster, G. T., and Toksöz, M. N., 1974a, Velocity and attenuation of seismic waves in two-phase media: Part I. Theoretical formulations: Geophysics, v. 39, no. 5, p. 587-606.

-, 1974b, Velocity and attenuation of seismic waves in two-phase media: Part II. Experimental results: Geophysics, v. 39, no. 5, p. 607-618.

Kvenvolden, K. A., 1993, Gas hydrates—geological perspective and global change: Reviews of Geophysics, v. 31, no. 2, p. 173-187.

Lee, M. W., and Collett, T. S., 2009, Gas hydrate saturations estimated from fractured reservoir at Site NGHP-01-10, Krishna-Godavari Basin, India: J. Geophys. Res., v. 114, p. B07102.

Lewis, R., Ingraham, D., Pearcy, M., Williamson, J., Sawyer, W., and Frantz, J., 2004, New Evaluation Techniques for Gas Shale Reservoirs: Schlumberger Reservoir Symposium.

Lonergan, L., and Cartwright, J. A., 1999, Polygonal faults and their influence on deep-water sandstone reservoir geometries, Alba Field, United Kingdom Central North Sea: AAPG bulletin, v. 83, no. 3, p. 410-432.

Loucks, R. G., Reed, R. M., Ruppel, S. C., and Jarvie, D. M., 2009, Morphology, genesis, and distribution of nanometer-scale pores in siliceous mudstones of the Mississippian Barnett Shale: Journal of Sedimentary Research, v. 79, no. 12, p. 848-861.

Lucier, A. M., Hofmann, R., Bryndzia, T., , 2010, Evaluation of variable gas saturation of acoustic log data from the Haynesville Shale gas play, NW Louisiana, USA: The Leading Edge.
Makogon, I. U. r. F., and Cieslewicz, W., 1981, Hydrates of natural gas, PennWell Books Tulsa, Oklahoma.
Mavko, G., Mukerji, T., and Dvorkin, J., 2009, The rock physics handbook: Tools for seismic analysis of porous media, Cambridge university press.
McGlade, C., Speirs, J., and Sorrell, S., 2013, Unconventional gas–A review of regional and global resource estimates: Energy, v. 55, p. 571-584.
Palaz, I., and Marfurt, K. J., 1997, Carbonate seismology, SEG Books.
Peebles, R., 2012, Integrating Seismic, Microseismic and Engineering Data to Optimize Lateral Placement and Completion Design in the Eagle Ford, Search and Discovery Article #80251 (2012).
Price, N. J., and Cosgrove, J. W., 1990, Analysis of geological structures, Cambridge University Press.
Reed, R., Loucks, R., and Milliken, K., Heterogeneity of shape and microscale spatial distribution in organic-matter-hosted pores of gas shales, *in* Proceedings AAPG Annual Convention and Exhibition, abstract2012, Volume 1236631.
Rich, J., and Ammerman, M., Unconventional geophysics for unconventional plays, *in* Proceedings SPE Unconventional Gas Conference2010, Society of Petroleum Engineers.
Riedel, M., Collett, T. S., and Shankar, U., 2011, Documenting channel features associated with gas hydrates in the Krishna-Godavari Basin, offshore India: Marine Geology, v. 279, no. 1-4, p. 1-11.
Røgen, B., Fabricius, I. L., Japsen, P., Høier, C., Mavko, G., and Pedersen, J. M., 2005, Ultrasonic velocities of North Sea chalk samples: influence of porosity, fluid content and texture: Geophysical Prospecting, v. 53, no. 4, p. 481-496.
Ryseth, A., Fjellbirkeland, H., Osmundsen, I. K., Skålnes, Å., and Zachariassen, E., 1998, High-resolution stratigraphy and seismic attribute mapping of a fluvial reservoir: Middle Jurassic Ness Formation, Oseberg Field: AAPG bulletin, v. 82, no. 9, p. 1627-1651.
Sayers, C. M., 2008, The elastic properties of carbonates: The Leading Edge, v. 27, no. 8, p. 1020-1024.
-, 2013, Introduction: Rock Physics for Reservoir Exploration, Characterisation and Monitoring: Geophysical Prospecting, v. 61, no. 2, p. 251-253.
Scholle, P. A., and Foundation, A. A. o. P. G., 1978, A color illustrated guide to carbonate rock constituents, textures, cements, and porosities, American Association of Petroleum Geologists.
Seljom, P., 2010, Unconventional Oil & Gas Production: Energy Technology Systems Analysis Programme
Sholl, D., and Hart, P., 1993, Velocity and amplitude structure on seismic-reflection profiles–possible massive gas-hydrate deposits and underlying gas accumulations in the Bering Sea: The Future of Energy Gases, US Geo: Surv. Prof. paper, v. 1570.

Slatt, R. M., and O'Brien, N. R., 2011, Pore types in the Barnett and Woodford gas shales: Contribution to understanding gas storage and migration pathways in fine-grained rocks: AAPG bulletin, v. 95, no. 12, p. 2017-2030.
Sondergeld, C. H., Ambrose, R. J., Rai, C. S., and Moncrieff, J., Micro-structural studies of gas shales, *in* Proceedings SPE Unconventional Gas Conference2010, Society of Petroleum Engineers.
Storvoll, V., and Brevik, I., 2008, Identifying time, temperature, and mineralogical effects on chemical compaction in shales by rock physics relations: The Leading Edge, v. 27, no. 6, p. 750-756.
Sukmono, S., 2010, Fundamental Issues on the Application of Seismic Methodologies for Carbonate Reservoir Characterization.
Tanikawa, W., and Shimamoto, T., 2006, Klinkenberg effect for gas permeability and its comparison to water permeability for porous sedimentary rocks: Hydrol. Earth Syst. Sci. Discuss., v. 3, no. 4, p. 1315-1338.
Toksöz, M. N., Cheng, C. H., and Timur, A., 1976, Velocities of seismic waves in porous rocks: Geophysics, v. 41, no. 4, p. 621-645.
Vanorio, T., and Mavko, G., 2011, Laboratory measurements of the acoustic and transport properties of carbonate rocks and their link with the amount of microcrystalline matrix: Geophysics, v. 76, no. 4, p. E105-E115.
Vernik, L., and Liu, X., 1997, Velocity anisotropy in shales: A petrophysical study: Geophysics, v. 62, no. 2, p. 521-532.
Wang, H., Sun, S. Z., Yang, H., Gao, H., Xiao, Y., and Hu, H., 2011, The influence of pore structure on P-& S-wave velocities in complex carbonate reservoirs with secondary storage space: Petroleum Science, v. 8, no. 4, p. 394-405.
Wang, Z., Hirsche, W. K., and Sedgwick, G., 1991, Seismic Velocities In Carbonate Rocks: Journal of Canadian Petroleum Technology, v. 30, no. 02, p. 112-122.
Winters, W. J., Pecher, I. A., Waite, W. F., and Mason, D. H., 2004, Physical properties and rock physics models of sediment containing natural and laboratory-formed methane gas hydrate: American Mineralogist, v. 89, no. 8-9, p. 1221-1227.
Wood, W. T., Stoffa, P. L., and Shipley, T. H., 1994, Quantitative detection of methane hydrate through high-resolution seismic velocity analysis: Journal of Geophysical Research: Solid Earth (1978–2012), v. 99, no. B5, p. 9681-9695.
Wyllie, M., Gregory, A., and Gardner, G., 1958, An experimental investigation of factors affecting elastic wave velocities in porous media: Geophysics, v. 23, no. 3, p. 459-493.
Xu, S., and Payne, M. A., 2009, Modeling elastic properties in carbonate rocks: The Leading Edge, v. 28, no. 1, p. 66-74.
Xu, S., and White, R. E., 1995, A new velocity model for clay-sand mixtu res: Geophysical prospecting, v. 43, no. 1, p. 91-118.
Zhao, L., Geng, J., and Han, D., Petrophysical Characterization of Pore Type in Tight Gas Carbonates of Southwestern China, *in* Proceedings 73rd EAGE Conference & Exhibition2011.
Zou, C., 2012, Unconventional petroleum geology, Newnes.
Zou, C., Yang, Z., Tao, S., Yuan, X., Zhu, R., Hou, L., Wu, S., Sun, L., Zhang, G., and Bai, B., 2013, Continuous hydrocarbon accumulation over a large area as a

distinguishing characteristic of unconventional petroleum: The Ordos Basin, North-Central China: Earth-Science Reviews, v. 126, p. 358-369.

FIGURES

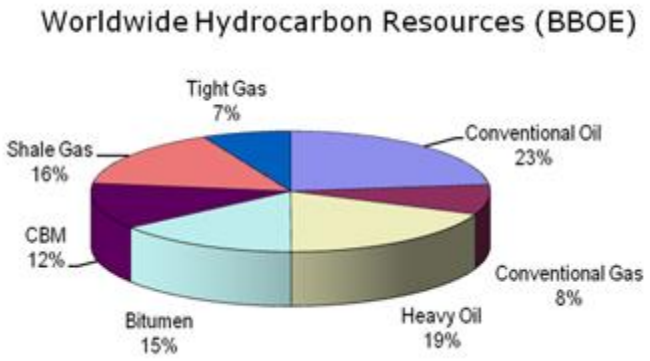

Figure 1: Volumetric productivity of hydrocarbon reservoirs. The percentages of unconventional resources are more than two third of the total worldwide hydrocarbon resources. Discovering unconventional reservoirs is growing intensely. Although production of hydrocarbon reservoirs has been growing by employing new technology, it is more challenging in unconventional reservoirs compared to the conventional ones. The difficulty of hydrocarbon production from unconventional reservoirs is due to inhomogeneity and complexity of grain arrangement (CGG-Website, 2014).

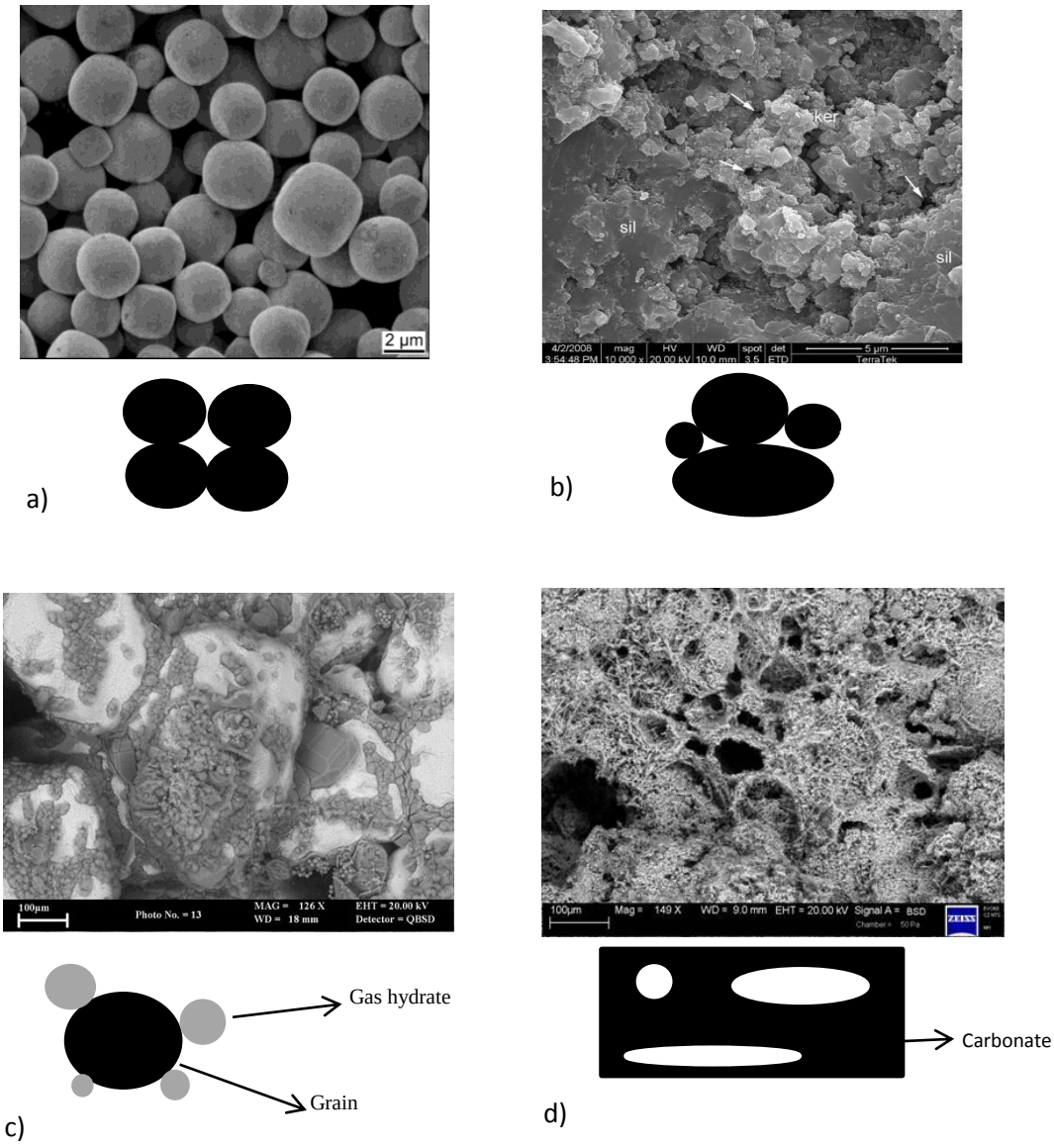

Figure 2: Grain arrangement comparison. Figures 'a' to 'd' respectively present the SEM images of (a) homogeneous reservoir, (b) Woodford Shale, (c) gas hydrate, and (d) carbonate reservoirs. (b) SEM image Woodford Shale formation from Canadian County, OK that contains 76% quartz and 18% clay (based on XRD data) and intercrystalline porosity. (c) Gas hydrate (darker color) coating sand grains (lighter color). (d) SEM photomicrograph showing the diversity of pore shapes in carbonate rock (Ernstson et al., 2011). Schematic diagram of grain arrangement for each case is shown below each SEM image. A mechanistic replication of grains and pore spaces can be achieved by applying a simple rock physics model (figure 3).

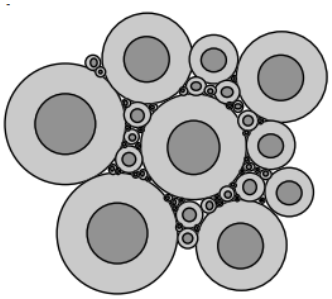

Figure 3: Model assumptions. In this figure, physical interpretation (schematic model) of grain arrangements of two-phase material for Hashin-Shtrikman (HS) model is shown. If the outer shell is the stiffer mineral, the model will produce the stiffest possible combination of the minerals. Otherwise, the softest possible combination is generated. These introduced maximum and minimum are known as the upper and lower boundaries of the model. Of course the upper (maximum) and Lower (Minimum) boundaries are dependent to the elastic moduli of the minerals (figure 4).

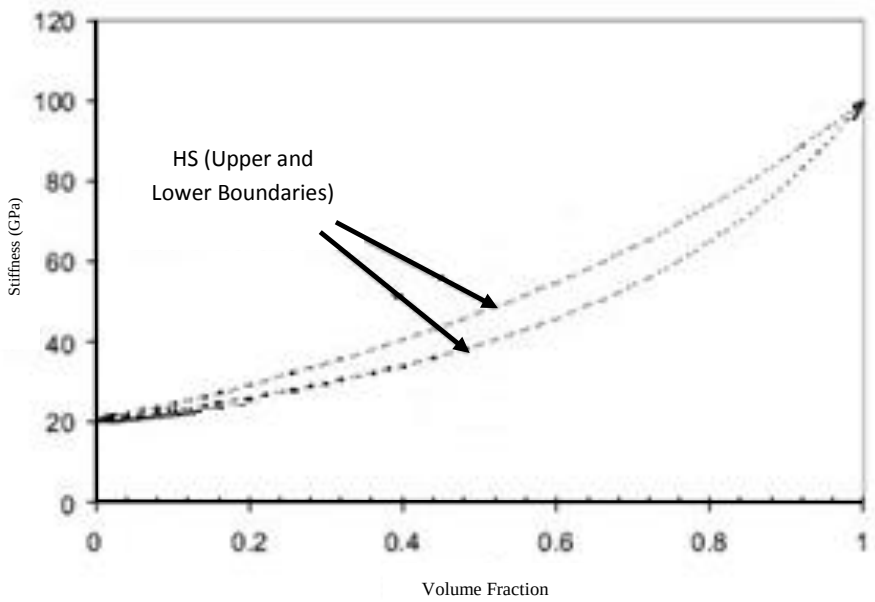

Figure 4: Models trajectories. The figure presents the upper and lower boundaries of HS model for a two-phase dry mineral. The start and end points of trends are known as end-members. Larger differences in elastic properties of the constituents will result in greater distances between the upper and lower boundaries (Mavko et al., 2009).

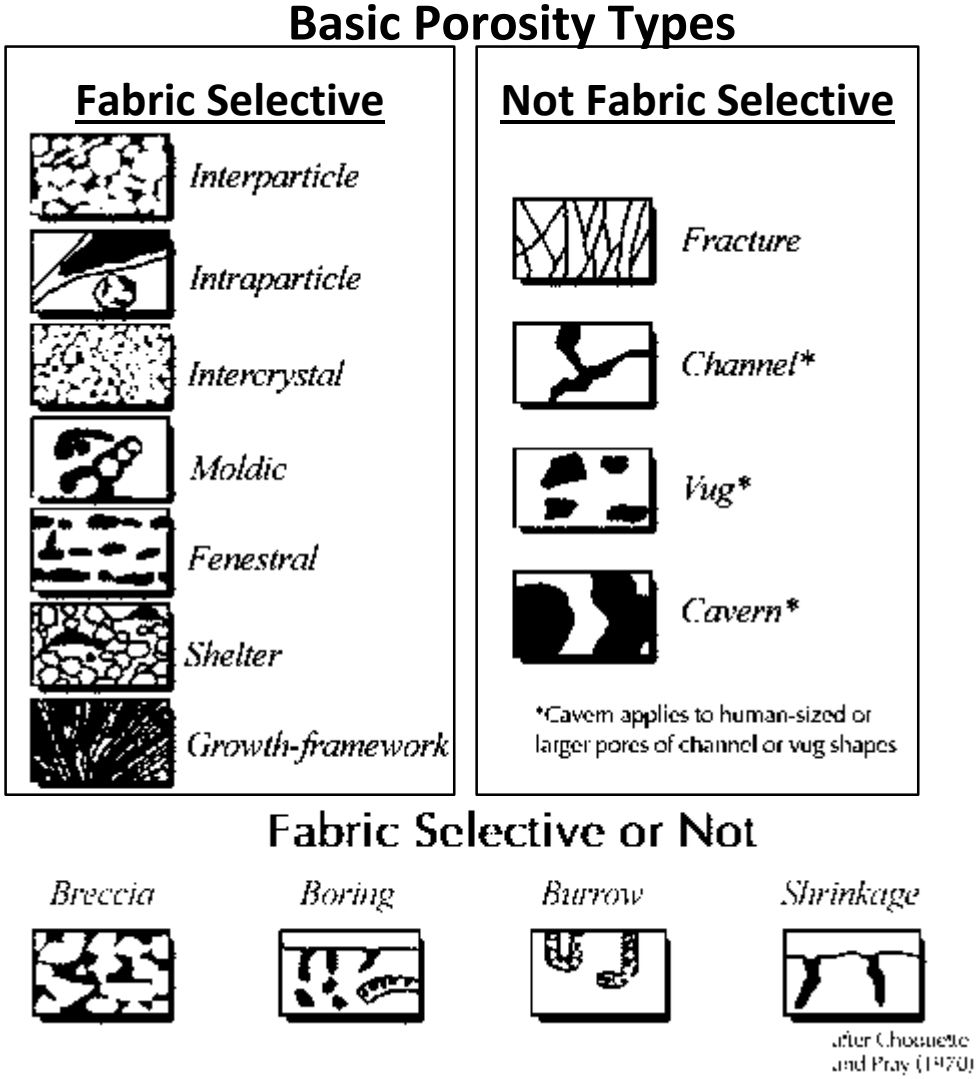

Figure 5: Basic porosity types. The figure represents the classification of porosity types (Choquette and Pray, 1970)

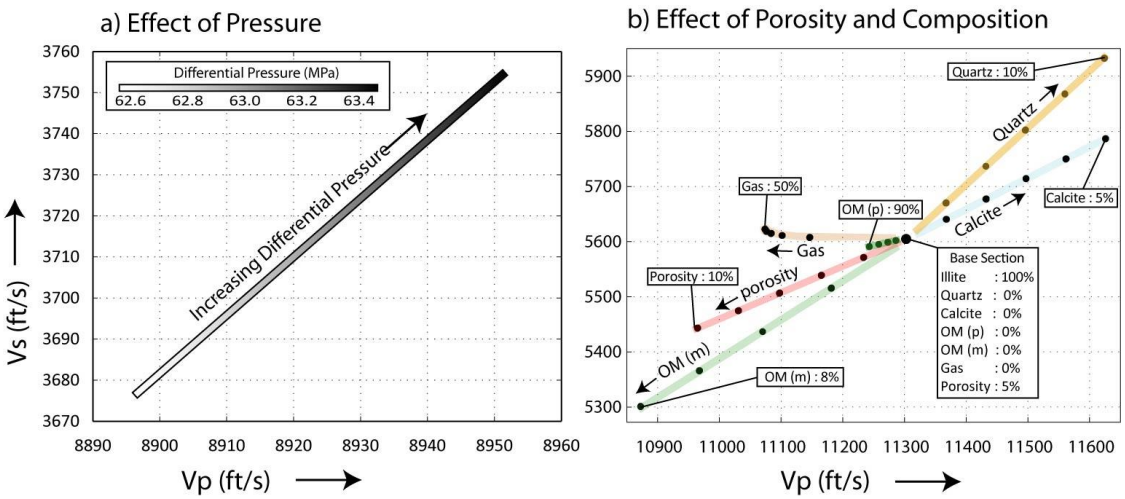

Figure 6: Stiff-Sand model behavior. (a) Sonic velocity (Vs vs. Vp) changes by increasing overburden pressure on 170ft thick "Base Section". The base section is 100 % clay (Illite) with 5 % ϕ and saturation of oil and gas are 0% out of total ϕ. (b) Effects of increasing calcite, quartz, gas, OM and ϕ are shown in this figure. Blue line: Increasing calcite causes increasing elastic velocity, Orange line: increasing elastic velocity due to quartz content. With quartz Vs increases faster compared to Vp. Brown line: increasing gas gradually increases Vs, but markedly decreases Vp. Effect of gas injection into water or oil saturated reservoirs is explained in detail by (Cardona et al. (2001)). Red and green lines show effects of increasing ϕ and OM on sonic velocities. If OM is assumed to be part of the fluid, it will not dramatically change elastic velocities. However, increasing OM as part of matrix significantly decreases both Vp and Vs. In other words, elastic velocities are more sensitive to OM changes in the matrix versus OM variation in the pore fluid. Elastic velocity changes due to calcite, quartz, OM, and ϕ variations are linear, but non-linear due to Gas. Pressure effects on both Vp and Vs are negligible compared to effects introduced of a reuslt of changes in ϕ and composition.

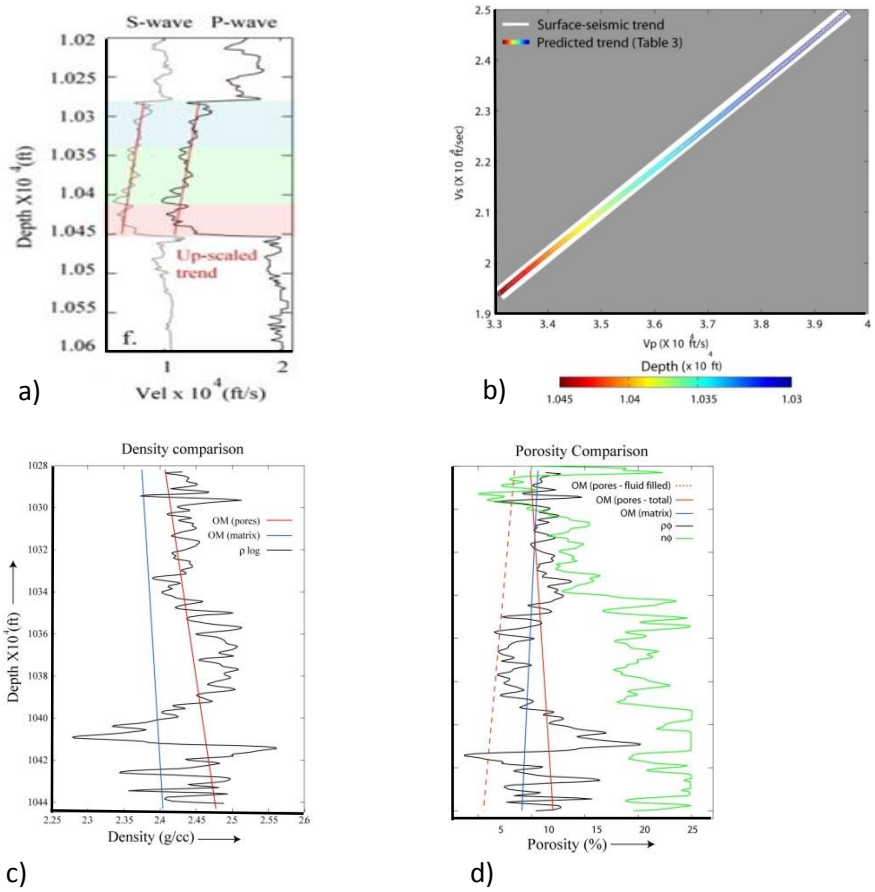

Figure 7: Application of Stiff-Sand model and its validity in the Woodford Shale. (a) dipole sonic velocities in black and gray colors and upscaled gradients (surface seismic trend, figure 6b); (b) comparison of predicted Vp-Vs trend and surface seismic trend is presented here. The white color presents the surface seismic data and its thickness is proportional to the standard deviations in the log data computed over 50ft depth interval and averaged over the entire Woodford. The colored overlay, is predicted Vp-Vs by optimal parameters over depth of Woodford Shale. (c) depicts comparison of density log with predicted density from the model. (d) displays comparison of $\rho\phi$ and nϕ with predicted porosity from the rock physics model. OM as part of matrix is shown by solid blue line. Solid red line describes OM as part of pore fluid. Also depicted is the fluid-filled ϕ (total ϕ - OM; dashed red). The ϕ and ρ is predicted from surface seismic and stiff-sand model.

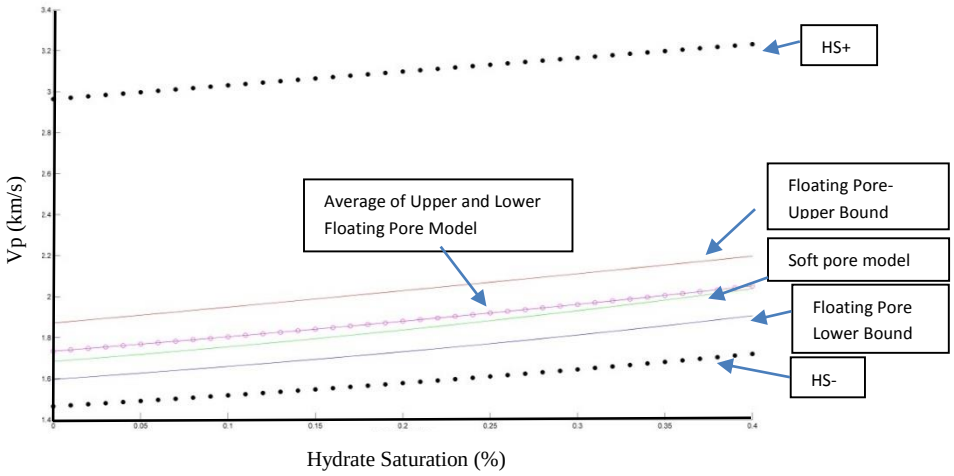

Figure 8: Floating pore model behavior. Gas hydrate saturation versus Vp. Predicted sonic velocities using floating pore model, HS and soft pore models are presented for a synthetic model with 20% quartz, 80% clay, 55% ϕ_t. gas hydrate is replaced with brine (which is the only pore fluid) at the ϕ_t ranging from 0 to 40% of. The upper and lower bounds of the floating pore model are closer to each other than HS. Therefore, the velocity will be in a narrower (more confined) range using the new model compared to the HS model. Results of soft pore model, is almost the same as average of upper and lower floating pore model. The gas hydrate in soft pore model is preserved within the void spaces. However in floating pore model, the gas hydrate saturation within ϕ_f or ϕ_M is distinguishable; in this example, gas hydrate is preserved within the ϕ_f.

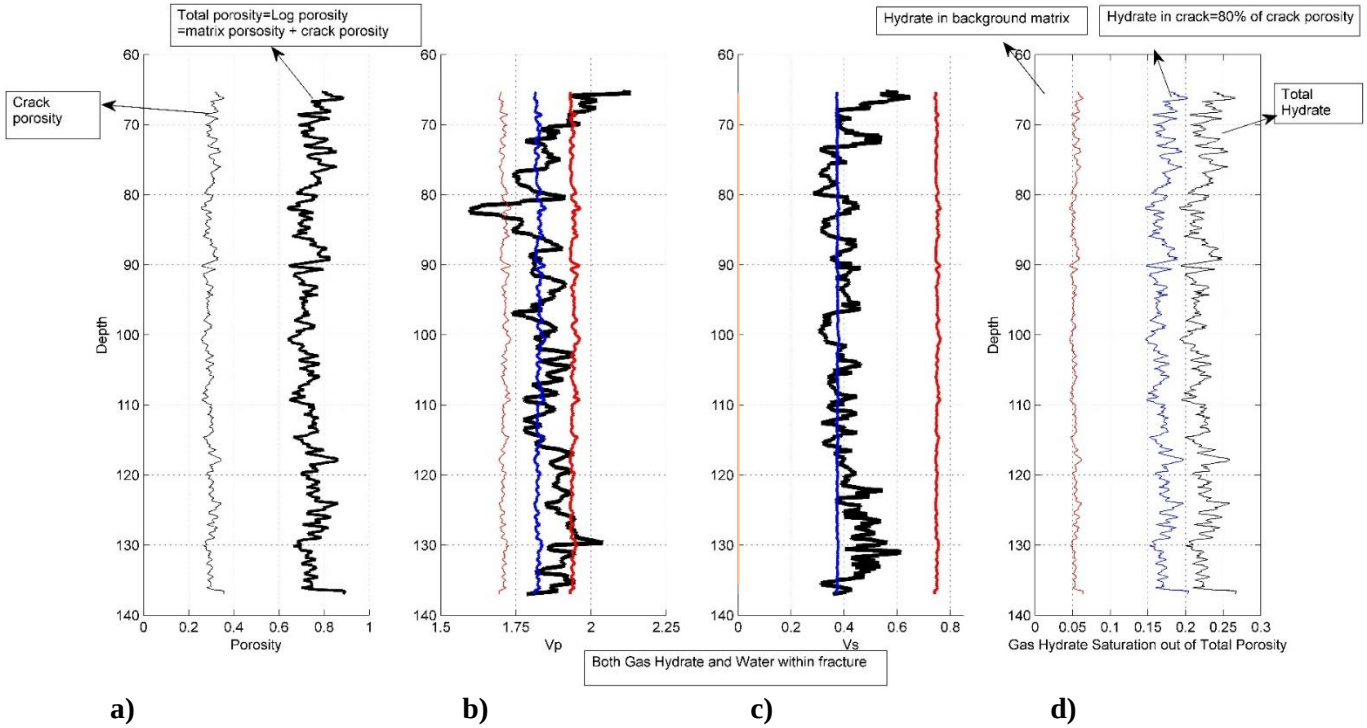

Figure 9: Application of floating pore model. a) applied ϕ_f and ϕ_t in the floating pore model is shown versus depth; b and c) sonic velocities obtained from dipole sonic log (black line), upper and lower bound and the average of upper and lower bounds of floating pore model (red, pink, and blue colors) are presented; d) applied gas hydrate saturation within ϕ_f, ϕ_M and ϕ_t are depicted in pink, blue and black colors, respectively.

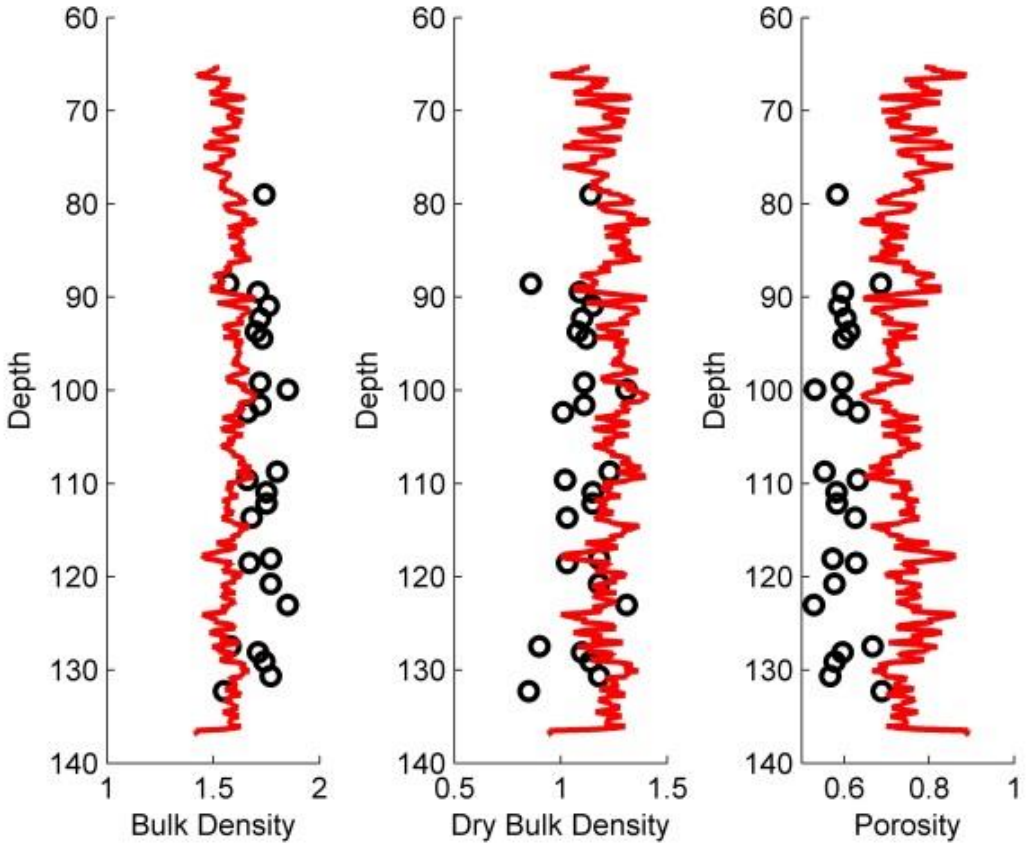

a) b) c)

Figure 10: Validity of floating pore model. a) bulk densities vs. depth, b) dry bulk densities vs. depth, and c) porosities vs. depth, which are applied in the model. The measured data from core are represented by black circles. The predicted values from the model are shown by solid red lines.

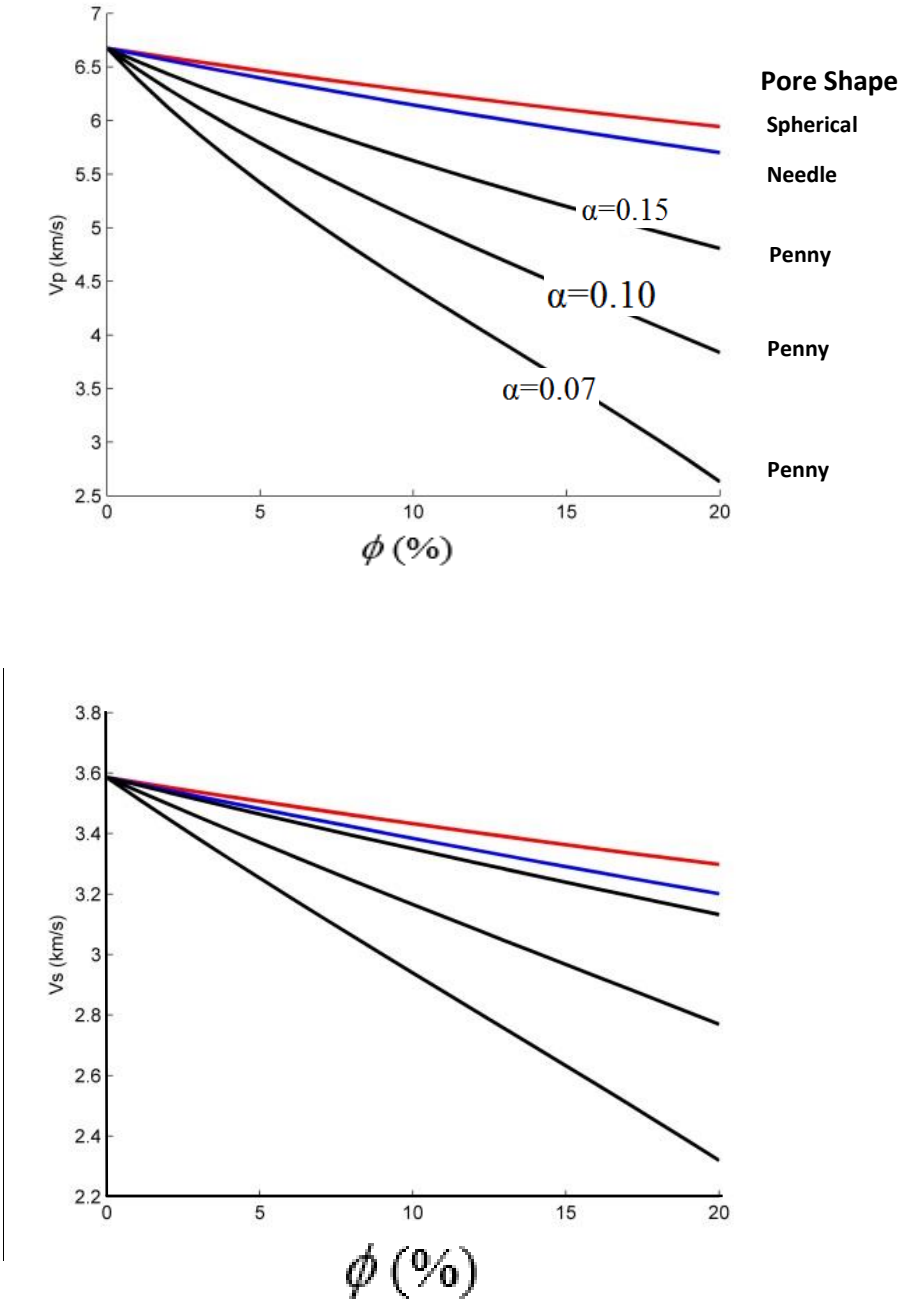

Figure 11: Kuster and Toksöz model behavior. In this figure, the Kuster-Toksoz model predicts Vp and Vs by increasing ϕ for different pore aspect ratio. For example, at the ϕ value of 15%, the Vp varies from 3.5 km/s to 6.3 km/s which, respectively corresponds to α around 0.07 (penny shape) to 1 (sphere shape).

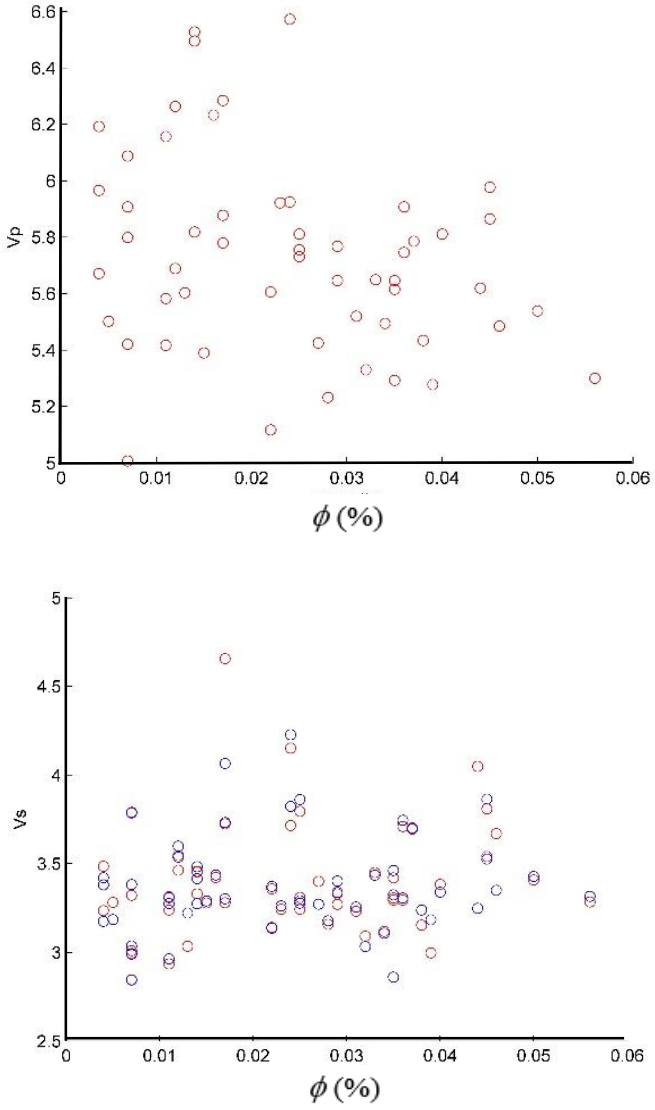

Figure 12: Scatted sonic velocity data. Scatted Vp and Vs of carbonate rocks are respectively presented in figure ‘a’ and ‘b’

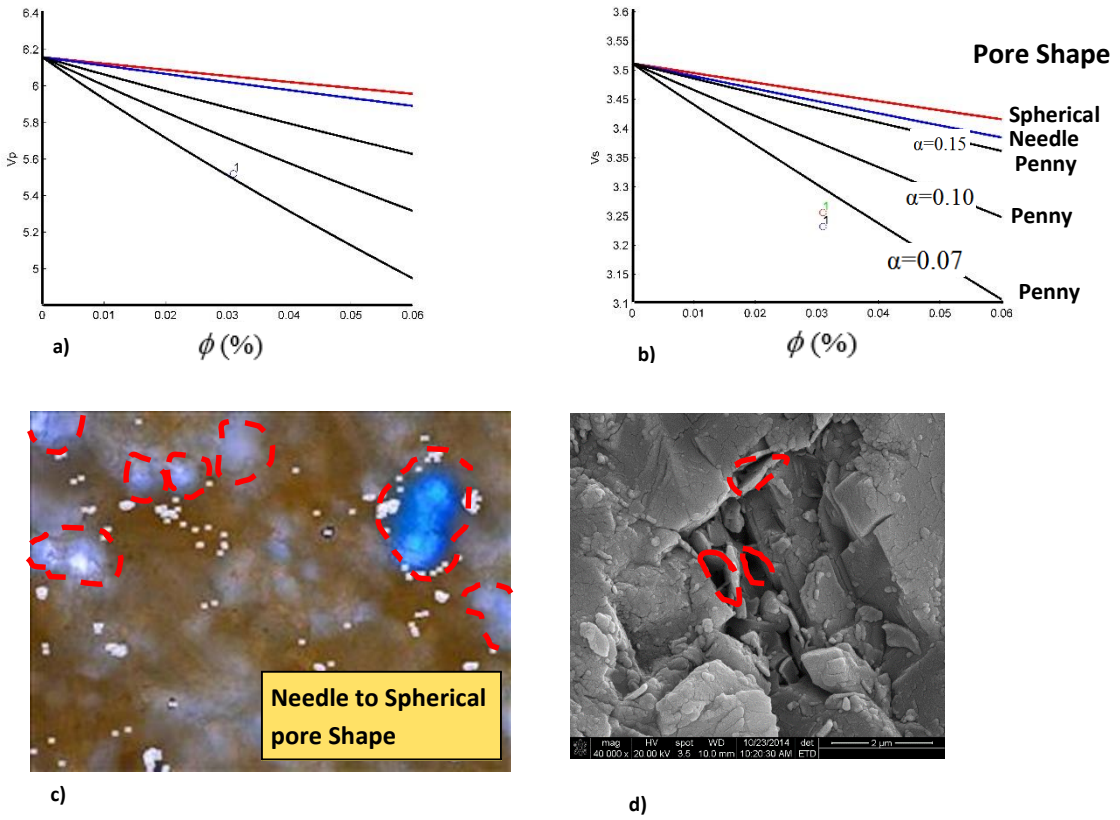

Figure 13: Application of Kuster and Toksöz model. Comparison of sonic velocities predicted by "Kuster and Toksöz" model and measured in the laboratory for one sample. Vs ('b') is computed in two different directions. Thin section ('c') and SEM ('d') images confirm validity of the predicted pore shape from the model. For this sample, pore aspect ratio is around 0.07.

VITA

POUYAN LIALEKOL, EBRAHIMI

Candidate for the Degree of

Master of Science

Thesis: MECHANISTIC MODELS of UNCONVENTIONAL RESERVOIRS

Major Field: Geology

Biographical:

Education:

Completed the requirements for the Master of Science in Geology at Oklahoma State University, Stillwater, Oklahoma in December, 2014.

Completed the requirements for the Master of Science in Petroleum Exploration Engineering at Sahand University of Technology, Tabriz, Iran in 2011.

Completed the requirements for the Bachelor of Science in Petroleum Exploration Engineering at Petroleum University of Technology, Abadan, Iran in 2008.

Publications:

Journal Papers

- P. Jaiswal, B. Varacchi, P. Ebrahimi, J. Dvorkin, J. Puckette, "Can Seismic Velocities Predict Sweet Spots in the Woodford Shale? A case study from McNeff 2-28 Well, Grady County, Oklahoma," *J. of Applied Geophysics,* (104), 26-34, 2014
- P. Ebrahimi, M. Oskouei, N. Keshavarz, S. Ismaeili, "Seismic Attributes Integration by GIS for Fracture Detection," *Energy Sources, Part A: recovery, Utilization, and Environment Effects,* (36), 9, 974-981, 2014
- P. Ebrahimi, M. Razavi, S. Ismaeili, M. Azarpour, "Gas Chimney Detection in 3D Seismic Data Using Supervised and Unsupervised Neural Network," *J.* of *Petroleum Science and Technology,* (31), 1188–1195, 2013

Expanded Abstracts

- P. Ebrahimi, P. Jaiswal, "Enhancement of Sub-Basalt Stratigraphy of Fareo-Shetland Basin Using Directional-Filter," *SEG International Exposition and 84th Annual Meeting,* 1570-1574, 2014
- P. Ebrahimi, B. Vanden Berg, P. Jaiswal, M. Grammer, J. Puckette, "Rock Physics Model of Mississippian Carbonate Rocks," *17th Annual AAPG/SEG Student Expo,* 2014
- P. Ebrahimi, P. Jaiswal, S. Harimkar, J. Puckette, "Mechanical Properties of Mississippian Rocks," *Mid-Continent AAPG Sectional Meeting,* Search and Discovery Article # 41239, 2013